

12-2009

# PRINCIPAL COMPONENT THERMOGRAPHY FOR STEADY THERMAL PERTURBATION SCENARIOS

Rohit Parvataneni

*Clemson University*, rparvat@clemson.edu

Follow this and additional works at: [https://tigerprints.clemson.edu/all\\_theses](https://tigerprints.clemson.edu/all_theses)

 Part of the [Engineering Mechanics Commons](#)

---

## Recommended Citation

Parvataneni, Rohit, "PRINCIPAL COMPONENT THERMOGRAPHY FOR STEADY THERMAL PERTURBATION SCENARIOS" (2009). *All Theses*. 702.

[https://tigerprints.clemson.edu/all\\_theses/702](https://tigerprints.clemson.edu/all_theses/702)

This Thesis is brought to you for free and open access by the Theses at TigerPrints. It has been accepted for inclusion in All Theses by an authorized administrator of TigerPrints. For more information, please contact [kokeefe@clemson.edu](mailto:kokeefe@clemson.edu).

PRINCIPAL COMPONENT THERMOGRAPHY FOR STEADY THERMAL  
PERTURBATION SCENARIOS

---

A Thesis

Presented to

The Graduate School of

Clemson University

---

In Partial Fulfillment

of the Requirements for the Degree

Master of Science

Mechanical Engineering

---

by

Rohit Parvataneni

December 2009

---

Accepted by:

Dr. Mohammad Omar, Committee Chair

Dr. Laine Mears

Dr. Steve Hung

## ABSTRACT

The work focuses on the qualitative enhancement of Thermographic Inspection data using Principal Component Analysis technique. A new processing tool named Economical Singular Value Decomposition (SVD) is proposed for analyzing the infrared image sequences acquired from the test specimen.

Experiments are carried out on test sample using thermal excitation modalities such as flash, halogen and induction to create temperature variations. The infrared (IR) image sequence containing the information about the sample is captured using IR cameras. The acquired IR image sequences are processed using the proposed Economical SVD which projects the matrix of raw pixel values of image sequence into a set of orthogonal components to extract features and reduce data redundancy. The results from processing revealed that Economical Singular Value Decomposition can be used with various thermal excitation modalities while enhancing the contrast between the defect and non defect areas. The proposed processing routine is benchmarked against the available standard techniques such as the Thermal Signal Reconstruction for one single application and specific experimental conditions.

**Keywords:** Thermographic Inspection, Principal Component Analysis, Economical Singular Value Decomposition, Orthogonal Components, Thermal Signal Reconstruction.

## **ACKNOWLEDGEMENTS**

I would like to acknowledge Dr. Mohammad Omar for his continuous help and support during this work. I would like to thank Dr. Laine Mears and Dr. Steve Hung for their valuable suggestions and comments that helped in improving the level of quality of this work.

Mr.N.Rajic is greatly acknowledged for his advice on the topic. Last but not the least I would like to thank my dearest friends Yi Zhou, Sree Harsha Pamidi, Konda Reddy, Suhas Vedula, Anupam Agarwal and Eric Planting for their help in my thesis review.

## TABLE OF CONTENTS

ABSTRACT .....	II
ACKNOWLEDGEMENTS .....	III
TABLE OF CONTENTS .....	IV
LIST OF FIGURES .....	V
LIST OF TABLES .....	X
CHAPTER 1 .....	1
1 INTRODUCTION .....	1
1.1 Non-Destructive Testing .....	1
1.2 Thermography .....	3
1.3 Classification of Thermography Techniques .....	5
1.4 Thermal Imaging Cameras .....	10
1.5 Thermal Properties of the Sample .....	12
1.6 Thermography Advantages and Limitations .....	14
CHAPTER 2 .....	16
2 PROCESSING ROUTINES FOR IR IMAGE SEQUENCES .....	16
2.1 Preprocessing Routines .....	16
2.2 Post-Processing Routines .....	18
2.3 Quantification criteria for processing .....	24
CHAPTER 3 .....	28
3 PRINCIPAL COMPONENT ANALYSIS .....	28
3.1 Literature Survey on Principal Component Analysis .....	28
3.2 Principal Component Analysis Method .....	32
3.3 PCT for Thermal Image Sequence .....	33
3.4 Singular Value Decomposition (SVD) based PCT Method .....	37
3.5 Singular Value Decomposition (SVD) for Thermal Image Sequence .....	37
CHAPTER 4 .....	40
4 ECONOMICAL SINGULAR VALUE DECOMPOSITION TECHNIQUE .....	40
4.1 Economical Singular Value Decomposition (SVD) for Thermal Image Sequence .....	41
CHAPTER 5 .....	46
5 LABORATORY TESTS .....	46
5.1 Test Specimen .....	46
5.2 Thermal Cameras .....	47
5.3 Heat Sources .....	48
5.4 Thermography using Flash as Heat Source .....	50
5.5 Thermography using Halogen as Heat Source .....	57
5.6 Thermography using Induction as Heat Source .....	64
CHAPTER 6 .....	71
CONCLUSION AND FUTURE WORK .....	71
LIST OF REFERENCES .....	72

## LIST OF FIGURES

Figure	Page
1.2.1 Thermal Imaging Experiment Setup.....	4
1.3.1 Thermography Diagram .....	6
3.2.1 Flow diagram of PCA.....	33
3.3.1 Sequence of $N_t$ image frames each with $N_x$ and $N_y$ elements.....	34
3.4.1 Flow diagram of SVD based PCT. ....	38
3.5.1 2D raster matrix with image sequence.....	39
4.1.1 Flow diagram of Economical SVD.....	41
4.1.2 Sequence of $N_t$ image frames each with $N_x$ and $N_y$ elements.....	42
4.1.3 2D raster matrix with $N_t$ rows and $N_x N_y$ columns.....	44
4.1.4 2D raster matrix with $N_x N_y$ rows and $N_t$ columns... ..	45
5.1.1 Test Sample black painted... ..	46
5.1.2 Test Sample unpainted.....	46
5.3.1 Halogen Heating Source.....	48
5.3.2 Flash Heating Source.....	49
5.3.3 Induction Heating Source.....	50
5.3.4 Various induction coils.....	50
5.3.5 Induction coil specifications.....	50
5.4.1 Flash Heating Source Experiment.....	51
5.4.2 Economical SVD based PCT Processing and Results of test sample using Flash Heat Source.....	52
5.4.2a ROI of Economical SVD based PCT.....	52
5.4.2b Raw image before processing using Economical SVD based PCT.....	52

5.4.2c	Result image of Economical SVD based processing.....	52
5.4.3a	Raw image with line profile before processing .....	52
5.4.3b	Raw image intensity profile before processing using Economical SVD based PCT.....	52
5.4.3c	Result image with line profile after Economical SVD based PCT processing .....	53
5.4.3d	Result image intensity profile after processing using Economical SVD based PCT processing .....	53
5.4.4	SVD based PCT Processing and Results of test sample using Flash Heat Source.....	53
5.4.4a	ROI of SVD based PCT.....	53
5.4.4b	Raw image before processing using SVD based PCT.....	53
5.4.4c	Result image of SVD based processing.....	53
5.4.5a	Raw image with line profile before processing .....	54
5.4.5b	Raw image intensity profile before processing using SVD based PCT.....	54
5.4.5c	Result image with line profile after SVD based PCT processing .....	54
5.4.5d	Result image intensity profile after processing using SVD based PCT processing .....	54
5.4.6	TSR Processing and Results of test sample using Flash Heat Source.....	55
5.4.6a	ROI of TSR.....	55
5.4.6b	Raw image before processing using TSR.....	55
5.4.6c	Result image of TSR processing.....	55
5.4.7a	Raw image with line profile before processing .....	56
5.4.7b	Raw image intensity profile before processing using TSR.....	56

5.4.7c	Result image with line profile after TSR processing .....	56
5.4.7d	Result image intensity profile after processing using TSR processing.....	56
5.5.1	Halogen Heating Source Experiment.....	58
5.5.2	Economical SVD based PCT Processing and Results of test sample using Halogen Heat Source.....	58
5.5.2a	ROI of Economical SVD based PCT.....	58
5.5.2b	Raw image before processing using Economical SVD based PCT.....	58
5.5.2c	Result image of Economical SVD based processing.....	58
5.5.3a	Raw image with line profile before processing .....	59
5.5.3b	Raw image intensity profile before processing using Economical SVD based PCT.....	59
5.5.3c	Result image with line profile after Economical SVD based PCT processing .....	59
5.5.3d	Result image intensity profile after processing using Economical SVD based PCT processing .....	59
5.5.4	SVD based PCT Processing and Results of test sample using Halogen Heat Source.....	60
5.5.4a	ROI of SVD based PCT.....	60
5.5.4b	Raw image before processing using SVD based PCT.....	60
5.5.4c	Result image of SVD based processing.....	60
5.5.5a	Raw image with line profile before processing .....	61
5.5.5b	Raw image intensity profile before processing using SVD based PCT.....	61
5.5.5c	Result image with line profile after SVD based PCT processing .....	61
5.5.5d	Result image intensity profile after processing using SVD based PCT processing .....	61



5.5.6	TSR Processing and Results of test sample using Halogen Heat Source.....	62
5.5.6a	ROI of TSR.....	62
5.5.6b	Raw image before processing using TSR.....	62
5.5.6c	Result image of TSR processing.....	62
5.5.7a	Raw image with line profile before processing .....	62
5.5.7b	Raw image intensity profile before processing using TSR.....	62
5.5.7c	Result image with line profile after TSR processing .....	63
5.5.7d	Result image intensity profile after processing using TSR processing.....	63
5.6.1	Economical SVD based PCT Processing and Results of test sample using Induction Heat Source.....	65
5.6.1a	ROI of Economical SVD based PCT.....	65
5.6.1b	Raw image before processing using Economical SVD based PCT.....	65
5.6.1c	Result image of Economical SVD based processing.....	65
5.6.2a	Raw image with line profile before processing .....	65
5.6.2b	Raw image intensity profile before processing using Economical SVD based PCT.....	65
5.6.2c	Result image with line profile after Economical SVD based PCT processing .....	66
5.6.2d	Result image intensity profile after processing using Economical SVD based PCT processing .....	66
5.6.3	SVD based PCT Processing and Results of test sample using Induction Heat Source.....	66
5.6.3a	ROI of SVD based PCT.....	66
5.6.3b	Raw image before processing using SVD based PCT.....	66
5.6.3c	Result image of SVD based processing.....	66

5.6.4a	Raw image with line profile before processing .....	67
5.6.4b	Raw image intensity profile before processing using SVD based PCT.....	67
5.6.4c	Result image with line profile after SVD based PCT processing .....	67
5.6.4d	Result image intensity profile after processing using SVD based PCT processing .....	67
5.6.5	TSR Processing and Results of test sample using Induction Heat Source.....	68
5.6.5a	ROI of TSR.....	68
5.6.5b	Raw image before processing using TSR.....	68
5.6.5c	Result image of TSR processing.....	68
5.6.6a	Raw image with line profile before processing .....	69
5.6.6b	Raw image intensity profile before processing using TSR.....	69
5.6.6c	Result image with line profile after TSR processing .....	69
5.6.6d	Result image intensity profile after processing using TSR processing.....	69

## LIST OF TABLES

Table	Page
5-A Adhesive spots dimensions.....	47
5-B Test Sample unpainted.....	47
5-C Thermal Cameras Specifications .....	47
5-D Halogen Specifications. ....	48
5-E Flash Specifications .....	49
5-F Induction Specifications.....	50
5-G Flash image sequence settings and processing time of the processing routines .....	57
5-H Flash processing intensity calculations.....	57
5-I Halogen image sequence settings and processing time of the processing routines .....	63
5-J Halogen processing intensity calculations .....	64
5-K Induction image sequence settings and processing time of the processing routines .....	70
5-L Induction processing intensity calculations .....	70

## **Chapter 1**

### **1 Introduction**

The inspection of finished or semi-finished products within a manufacturing process chain aims at evaluating such products functionalities and its internal or subsurface structure. Several destructive and non-destructive modalities exist to achieve fast and reliable testing procedures that scan the product subsurface features or internal components. . In a destructive testing mode, the component is split into parts or subjected to high stresses to evaluate its quality. For example, a welded joint can be loaded in a tensile machine to record the stress at which the joint separates. Meanwhile, in the case of non-destructive testing we can detect, locate, measure, and evaluate facial and sub-facial flaws of the components without causing any damage or changing the integrity, of its properties, composition to avoid impairing its future usefulness and serviceability. Thus, non-destructive inspection can be done on 100% of the manufactured components. Several types of the Non-Destructive testing procedures are currently being used in the industry that include; ultrasonic testing, radiography, eddy current testing, magnetic inductive testing, acoustic emission and thermography. Each of these techniques has its own advantages and disadvantages that mainly relate to the testing system cost, speed, accuracy and safety.

#### **1.1 Non-Destructive Testing**

Non-Destructive Testing (NDT) modalities include all the inspection techniques that do not alter the inspected components properties or its usability once it has undergone the required testing steps. Current Non-Destructive applications include crack

detection, material properties analysis, delaminations and the material subsurface structure. Following paragraphs describe the most commonly used non-destructive testing methods; mainly Ultrasonic testing, Radiography, Acoustic emission, Thermography.

### **Ultrasonic Testing:**

In ultrasonic testing a short pulse wave is sent into the component or material to be tested to detect internal flaws of material under inspection. Generally the wavelength of the ultrasonic waves used is 1 to 10mm, sound velocities of 1 to 10 Km/s is used and frequencies are generally within the range of 0.1 to 15 MHz, but there are applications in which 50 MHz frequency is also used [1]. The main advantage of ultrasonic testing is that it can penetrate into objects of very high thicknesses and the flaws can be easily distinguishable. The main disadvantage is that it requires the material to be homogenous, with uniform surface roughness, in addition it requires a medium to transmit the waves from the transducer into the bulk, additionally, ultrasound is a point inspection technique and can be time consuming for large areas.

### **Radiography:**

In radiography, the specimen shadow is generated using a penetrating radiation rays such as gamma or x-ray [1]. The images are recorded using x-rays on the film called as radiograms. The recorded radiograms have different contrast levels depending on the flaws, thickness, densities and the nature of its chemical composition. The radiograms require access from both sides of the specimen being tested because, it operates based on a transmission mode.

### **Acoustic Emission Testing:**

Acoustic Emission is the phenomenon of sound generation in materials when they are under stress. Most materials which are designed to withstand high stress levels emit acoustic energy when stressed. These pulse wave emissions have frequencies in the range of 1 KHz to 2 MHz or greater [1]. Acoustic emission is used to non-intrusively monitor structural integrity and characterize the behavior of materials when they undergo deformation, fracture or both. Unlike ultrasonic or radiography techniques, acoustic emission does not require external energy for inspection. Acoustic emission techniques have been used to monitor components and systems during processing, detecting and locating leaks, mechanical property testing, and testing pressurized vessels. One of the main problems with acoustic emission is that it produces large amount of data that needs to be stored and retrieved for analysis in addition to the lack of automation.

### 1.2 Thermography

Thermography which is well known as infrared thermography or thermal imaging captures the temperature variations emitted by a body using a radiation detector. The captured radiation can then be analyzed to retrieve information about the material subsurface thermal resistances, which is then used to understand its internal configuration. Also, such information helps in determining the presence or nature of defects in the body.

In the early years, thermal imaging was used as a secondary test to support primary inspection techniques such as radiography and ultrasonic because at that time, it was considered to be a non contact yet qualitative technique with poor data capture (resolution and frame rate) in addition to lack of dedicated signal processing techniques

[2]. But in the recent years with the advancements in the infrared cameras and data processing codes, thermal imaging is currently being used as a standalone technique for inspection of several samples types

As shown in the figure 1.2.1, in a general thermal imaging technique the test sample is either excited externally or the inherent radiation from the sample is captured using a thermal imaging camera. The captured infrared sequences are processed and stored in a computer. The stored sequences consist of unwanted noise, interference from the surroundings, reflection from the sample surface and other image disturbances, which are to be removed. The processing of the captured data is carried out to remove these undesirable signals from the infrared sequences and to clearly visualize the sample nature. Figure 1.2.1 provides general visualization of the process.

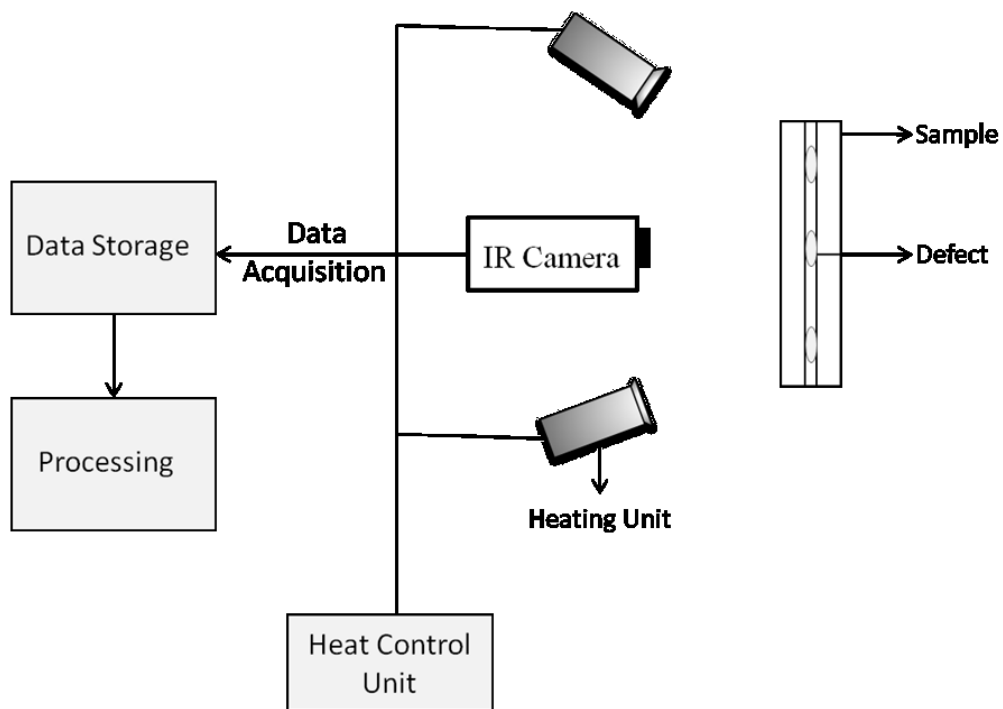


Figure 1.2.1 Thermal Imaging Experiment Setup

### 1.3 Classification of Thermography Techniques

Thermal Imaging can be classified into two main categories depending on the sample excitation:

1. Passive Thermography
2. Active Thermography

**Passive Thermography:** In passive thermography technique; the un-excited infrared radiation (natural emission) is used to test the sample quality and detect any defects in its structure. In passive thermography the temperature difference between a defect and its surroundings is used distinguish it [3].

**Active Thermography:** In active thermography an external source is used to excite the test sample thus creating temperature variation between the defective and non defective areas within the test sample. The excitation can be achieved through optical, electromagnetic, mechanical, thermo elastic heating and convection based heating or cooling. Each of these techniques are further divided into sub classes which are explained below and shown in figure 1.3.1.

**Optical Excitation:** In optical excitation, the test sample is externally heated using a heat source such as pulse or steady state. The optical excitation is further classified into pulse thermography and lock-in thermography also known as modulated thermography.



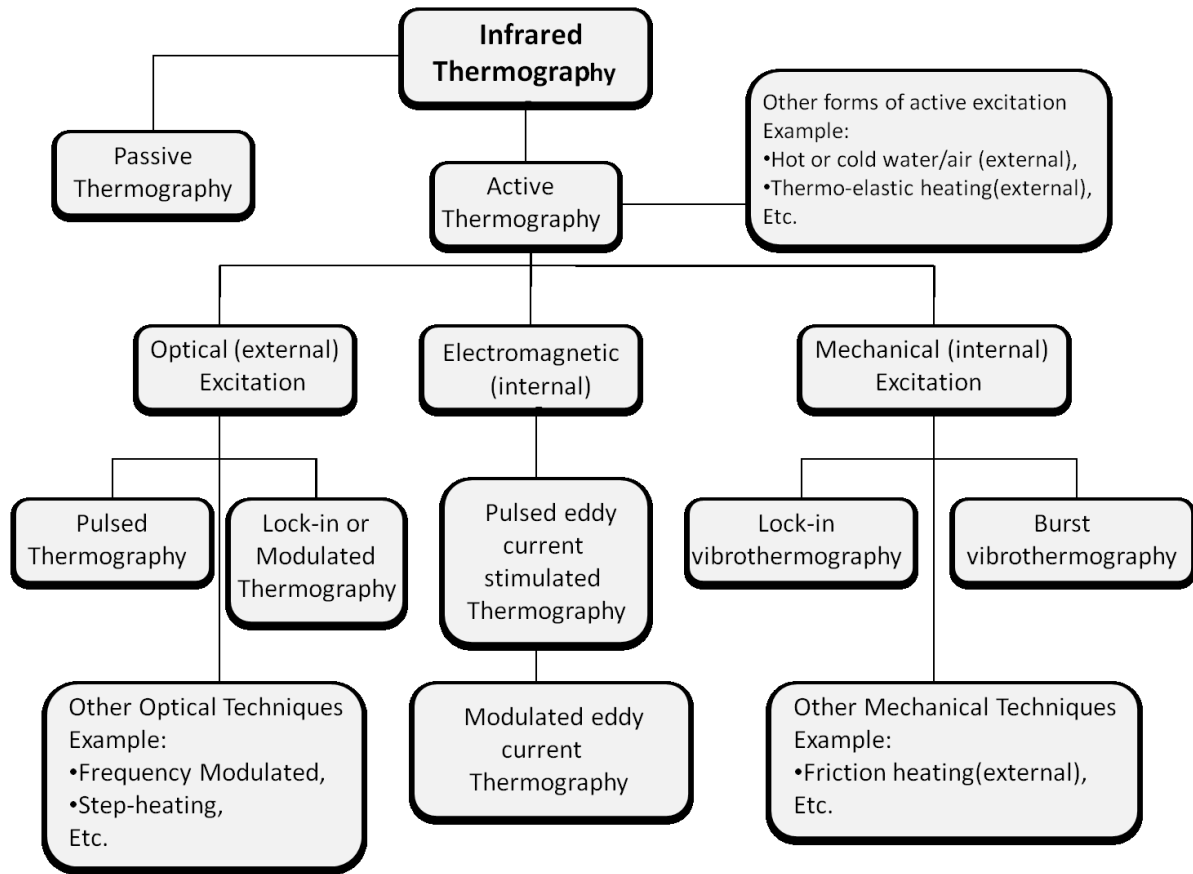


Figure 1.3.1 Thermography Diagram

**Pulse Thermography:** Pulse thermography or flash thermography is a widely used active thermography technique. Pulse thermography uses a short high energy, heat pulse that lasts for few milliseconds. The pulse heats the sample surface during the short duration of pulse [4]. The heat dissipates from the surface through the entire part as the surface begins to cool down. The dissipation of heat varies from the defect to non-defect area due to the difference in thermal resistances, which creates a temperature difference between the two areas. This temperature time history is then captured as a thermal sequence using a thermal imaging camera. These thermal sequences are later processed to better visualize the defects from their sound area. With the advancement of technology in the thermal cameras and the pulse heating sources, the pulse thermography has become

one of the mostly used thermography techniques as it provides us with precise and repeatable measurements for the test samples. The main drawbacks of pulse thermography is that it is effected by a variety of noises such as the reflection from the surroundings, surface emissivity variations, facial geometries, non uniform heating of the sample and the location of the heat source. The reflection problem cannot be reduced to a great extent as it depends on the sample surface roughness (reflectivity, color), material nature and its size. The non-uniform heating can be reduced to some extent by designing sample specific heat source and orienting heating source more towards the sample.

**Lock-in Thermography:** Lock-in thermography is well known as modulated thermography, it uses a periodic heat flux incident on the surface to excite the test sample and the local variations in amplitude and phase are synchronized for capturing through a lock-in amplifier. The main draw back with lock-in thermography is the long capture durations that are needed for defects at larger depths with very low modulation frequencies, also it requires additional hardware such as the lock-in amplifier and dedicated image acquisition controllers [5, 6].

In optically excited lock-in thermography a thermal wave source is used to generate a sinusoidal temperature modulation. A sinusoidal temperature modulation is used to thermally excite the sample so that the frequency and shape of the response are preserved. The heat source is designed so that the test sample is thermally excited at a required sinusoidal frequency depending on the nature of the sample being tested. The thermal wave is damped so that it penetrates the required depth inside the sample. The penetration depth of the sinusoidal wave also depends on its frequency. The thermal

wave penetrates deeper into sample at lower frequencies and hence a very low frequency wave can be used to inspect very thick and non-homogenous bulks [6].

The heat transfer phenomenon in the lock-in thermography is described in real and imaginary parts of the sinusoidal wave equation. The real and imaginary parts are given by the inverse of thermal diffusion length equation. The thermal diffusion length  $\mu$  of the test sample is given by equation 1.1[6],

$$\mu = \sqrt{\frac{\alpha}{\pi f}} \quad (1.1)$$

The thermal diffusion length  $\mu$  is a function of material thermal diffusivity  $\alpha$  and its wave frequency  $f$ . The thermal diffusivity of the material  $\alpha$  is given by equation 1.2 [8],

$$\alpha = \frac{\lambda}{\rho c_p} \quad (1.2)$$

where  $\rho$  is the density of the test sample,  $C_p$  is the specific heat capacity of the sample and  $\lambda$  is the thermal conductivity of the test sample. The depth range, for the amplitude image, is given by  $\mu$  and the maximum depth  $p$  that can be inspected using a specific configuration is calculated as  $1.8\mu$ .

**Electromagnetic Excitation:** In electromagnetic excitation, the eddy currents induce current circulation phenomena inside the test sample, which generates internal heat that later propagates to the surface. Magnetic induction is governed by the equation 1.3

$$\varepsilon = -\frac{d\Phi_B}{dt} \quad (1.3)$$

where  $\varepsilon$  is the electromotive force (EMF) in volts and  $\Phi_B$  is the magnetic flux through the circuit in Weber. The defect and the non-defect areas respond uniquely for the induced current and have different temperature difference due to magnetic excitation. This

temperature difference between the defect and non-defect areas is then captured using an infrared camera. The main disadvantage with the electromagnetic excitation is that it is applicable only to conductive materials [7].

**Mechanical Excitation:** Mechanical excitations of the test sample can be of two kinds such as internal and external excitations. The test sample is internally excited if it is excited using vibrothermography. The test sample is externally stimulated using excitation technique such as friction heating.

**Vibrothermography:** Vibrothermography is an internal excitation technique, where the sample is mechanically excited by sonic or ultrasonic oscillations. The test sample excitations are created by coupling an ultrasonic transducer to the sample. The propagation of ultrasonic waves into the material transforms the mechanical energy into thermal energy at crack tips. The energy dissipation between the defect and non-defect area is large due to friction effects between them. The difference in energy dissipation leads to difference in temperatures between the two areas which are then captured using an infrared camera. The vibrothermography is again classified into two categories such as lock-in vibrothermography and burst vibrothermography.

**Lock-in vibrothermography:** In lock-in vibrothermography the high frequency oscillation can be amplitude or a frequency modulated while the detection lock-in system is synchronized with the amplitude varying input signal to detect the amplitude and the phase of the surface temperature [8]. This surface temperature is recorded by an infrared camera.

**Burst vibrothermography:** Burst vibrothermography is also known as sonic infrared imaging. In the burst vibrothermography the sample is excited by a burst of ultrasonic pulse lasting for 50 to 200ms. This ultrasonic pulse creates a difference in the surface temperature between the defect and defect surrounding areas. This difference in surface temperature is recorded as function of time using an infrared camera [9].

#### 1.4 Thermal Imaging Cameras

##### **Infrared Thermography:**

Once the thermal excitation technique is selected, we need to decide on the suitable thermal imager and its settings (dynamic range, frame rate) to be used for capturing the infrared image sequences generated by the test sample. Thermal detector or thermal imaging camera is the heart of entire thermography technique. The thermal imaging cameras operate only in the infrared region. Such spectrum can be further classified into following [3]

- Near infrared                      1.5-3 $\mu\text{m}$
- Middle infrared                      3-5 $\mu\text{m}$
- Long wavelength                      8-13 $\mu\text{m}$
- Far infrared                      20-1000 $\mu\text{m}$

The thermal imaging cameras generate thermograms from the captured heat radiation. Such thermograms capture the temperature variations of the specimen with time and space. The Infrared radiations can be focused by appropriate optics and detected by

specially designed sensors. The IR cameras used to detect these radiations are classified in to two types:

- Un-cooled camera
- Cooled camera

#### **Un-cooled Infrared Camera:**

Un-cooled cameras have infrared detectors composed of micro-bolometric based arrays [10]. A temperature difference detected at the focal plane array is then converted into electrical signal output. The infrared radiation from the sample heat the sensors and a change in its physical properties change such as its electrical properties like resistance, voltage and current of the sensors. The changes in these properties are then scanned and then compared with the original values at the operating temperature of the sensor. In contrast to photon detectors, the thermal detectors operate at room temperature and hence no cooling is needed. But the absence of cooling systems make the un-cooled cameras less sensitive, increase the thermal response time, lower the spatial resolution and ultimately decrease the quality of the image. Though the un-cooled cameras have low sensitivity and slow response time they are cost-effective to build, maintain and easy to use.

#### **Cooled Infrared Camera:**

The current technologies used in the cooled cameras comprise infrared photon based focal plane arrays [10]. The infrared detectors are made of Indium Antimonide InSb, Indium Arsenide, Lead sulfide, and Lead selenide semi-conductors. Unlike their un-cooled counterparts, cooled cameras contain sealed cryogenic chambers. The function

of these chambers is to reduce the temperature of the focal plane array to a temperature much lower than that of the ambient air temperature [11]. Cryogenic cooling is required because at ambient temperature the signal is widely affected by thermal noise generated due to random generation of carriers in the semi-conductors. These detectors are cooled using liquid nitrogen or through Sterling's coolers with temperatures at 70K-80K. The cooling system enables the cooled detectors to have good signal to noise ratio at a high frame rate. The Noise Equivalent Temperature Difference (NETD) which is a measure of IR camera sensitivity is in the order of  $\mu\text{K}$  for the cooled cameras. The high spatial resolution of the cooled cameras allows it to provide high quality images. The advancements in the hardware used for the manufacture of thermal cameras have led to the improvements in the frame size and capture rate of the cameras which ultimately helped in the reducing the noise levels.

### 1.5 Thermal Properties of the Sample

The sample thermal properties also play an important role in deciding on the suitable thermography mode. The thermal properties controls how the test sample absorbs and emits thermal radiation incident on the surface. The thermal emission of solids is generally compared with black body emission. A black body absorbs the total radiation incident on it and hence appears black in color. The emissivity ( $\epsilon$ ) of a material is the capability of the material surface to emit heat radiation. It is a measure of a material's ability to radiate absorbed energy. The total emissivity of material is total energy radiated by a material at temperature T compared with the emission of black at the same temperature which is equal to 1 [12]. The emissivity of the material is always less than 1. The emissivity provides an accurate measure of how efficiently an object emits

infrared energy. The emissivity of metals is low, but increases with the increase in temperature. Some materials have emissivity values above 0.8 which tends to decrease with the increase in temperature. The emissivity of a material provides an accurate measure of how efficiently a body emits infrared energy. Because the sample surface can be easily modified, its emissivity can be improved by painting it with black paint, high emissivity coating or applying a black tape. Once the sample emissivity is enhanced, the absorption and thermal emission can be improved. The sample preparation will be least if the emissivity is high or need to be prepared as mentioned above to have better thermal emission from the surface.

The material thermal diffusivity also plays an important role in the thermography inspection technique [12]. The rate at which the incident heat propagates through the sample defines its thermal diffusivity. The materials with high thermal diffusivity propagate heat at high rates thus it is difficult to capture its temperature time history without high frame rate detectors. This increases the cost and complexity in the camera manufacture. The materials with medium diffusivity require simple heating elements, cameras and experimental setup

The material thermal effusivity also has an impact on the thermography inspection. Thermal effusivity is the square root of the product of thermal conductivity and heat capacity of the material [12]. Thermal effusivity is the thermal inertia of the material that resists the increase of temperature when heat is applied. Metals generate very weak infrared signals difficult to be captured by thermal cameras due to their high thermal effusivity.



The infrared image sequences captured by the infrared cameras are to be processed using various processing techniques such as thermal reconstruction, contrast enhancement, frame averaging and pulse phase to remove the noise, reflection and other surrounding disturbances that might have crept in as the inspection is carried out.

### 1.6 Thermography Advantages and Limitations

#### **Advantages of Thermography**

- Non contact method of inspection.
- Can be used to inspect very large parts in one single test.
- The duration of inspection is short.
- Capability to inspect different materials and composites.
- Can be applied to inspect intricate part geometries.
- Capability to inspect components of less accessibility
- Can be used in real time applications such as during production cycles.
- Easy to setup, use and maintain on a production line.

#### **Limitations of Thermography:**

- Dependence on the nature of heating source, duration of heating and location of heat source.
- Difficulty to inspect thick samples.
- Capture duration must be studied depending on the nature of material being tested.
- Performance of the infrared camera used has major impact on the capture quality.
- Surroundings of the test sample can impact the image capture.
- Need for sample to be heated uniformly.

- Specific excitation technique is needed for each application.
- Some techniques require the thickness of sample and nature, location of defect to be known.

## Chapter 2

### 2 PROCESSING ROUTINES FOR IR IMAGE SEQUENCES

The infrared image sequences from thermal cameras are to be processed automatically with least effort from the operator using thermography. But this capability is not achieved in the present available testing scenarios due to the presence of unwanted signals due to hardware limitations such as limitations from detectors used in the thermal cameras which generate dead pixels and image saturation due to effects from surroundings. To overcome all these problems and better visualize the defect and non-defect areas in the sample, the acquired infrared image sequences are to be enhanced through some preprocessing and post processing steps.

#### 2.1 Preprocessing Routines

The acquisition problems present in the captured thermal sequences caused by acquisition system are to be rectified before the actual processing is carried out for contrast enhancement. The problems from the acquisition system are rectified in the preprocessing phase of data analysis as discussed below.

##### **Fixed Pattern Noise:**

The thermal detectors in the thermal imaging cameras have slight variations in responsivity to the incoming radiation from the sample. This difference in responsivity to the incoming radiation from the test sample causes fixed pattern noise [15]. This is a common problem in the focal plane arrays used as infrared detectors. The fixed pattern noise can be eliminated by capturing an image from a black body in the particular test configuration used for inspecting the test samples. This image is later subtracted from the infrared image sequence of the test sample to eliminate fixed pattern noise.

**Bad pixels:**

An anomalous pixel in the image frame captured using an infrared detector behaving differently from the rest of the pixel arrays is defined as a bad pixel. The bad pixels are classified into two categories: i) Dead pixel ii) Hot pixel. A dead pixel in the image frame remains black or unlit and a hot pixel is permanently bright or white. The bad pixels are either dead or hot do not provide any useful information and only contribute to image contrast deterioration. The bad pixel count in some thermal cameras can be reduced by non uniformity correction carried out before inspection where the bad pixel values are altered by replacing them with average value of neighboring pixels.

**Vignetting:**

The darkening of images in the corners with respect to the image center of the captured image frames due to limited exposure is defined as vignetting. Vignetting is another source of noise which depends on both location and temperature difference of pixel corresponding to the ambient temperature [15].

**Temperature Calibration:**

The temperature calibration of a thermal camera is carried out using a polynomial transformation function. In the process of temperature calibration a reference heat source is selected whose temperature can be varied in steps. These temperature variations from the heat source are captured with the thermal camera as reference image sequences. These reference images are averaged and fit into the polynomial function used to calibrate the thermal camera. Once all the images acquired are curve fitted into the polynomial function, the calibration of camera is complete and can now be used for image acquisition.

### **Noise Filtering:**

Noise filtering is the most important preprocessing technique used on the acquired thermal image sequences from the thermal imaging cameras. Gaussian filtering is one of the techniques used to filter noise from the captured images as discussed in literature [15]. The resultant image sequences obtained after the noise filtering show better contrast difference between the defect and non defect areas in the sample.

After the completion of preprocessing of the captured infrared image sequences from the thermal camera the processed data is now applied with post processing routines to further enhance the image sequences and better distinguish the defect and non-defect areas.

## 2.2 Post-Processing Routines

The pre-processed data of the infrared thermal image sequences are post processed to further enhance the image sequences and to better distinguish the defect and non-defect areas. There are many post processing techniques available to process the infrared image sequences, some of which are discussed in detail in the following sections.

### **Thermal Contrast Techniques:**

Thermal contrast is the most common and simple technique used in the processing the thermographic sequences obtained after pre-processing. In this technique a non defect area in the sample also known as the sound area ( $S_a$ ) is located to calculate the absolute temperature contrast. Locating the sound area is the main drawback of the method as the results from the method vary with the location of the sound area of the sample. Once the sound area is located, the absolute temperature contrast is calculated using the equation 2.1 [5, 11]:

$$\Delta T(t) = T_d(t) - T_{S_a}(t) \quad (2.1)$$

with  $T_d$  as the temperature of the pixel or group of pixels in the defective area at time  $t$ ,  $T_{S_a}$  is the temperature of the pixel or group of pixels in the sound area at time  $t$  and  $\Delta T$  as the absolute thermal contrast for the defective pixel or group of pixels. No defect is detected at a particular time  $t$  if  $\Delta T(t)=0$ .

The problem of locating the sound area in the sample can be reduced by using differentiated absolute contrast (DAC) technique in which the first few images of the sample are used to locate ideal sound area ( $S_a$ ) temperature instead of locating the non-defect area to calculate sound area ( $S_a$ ) temperature [5, 11]. The technique assumes the absence of defect in the thermal sequence before the sample is thermally excited and the local temperature of the defect and non-defect area is same and is given by equation 2.2:

$$T_{S_a}(t') = T_d(t') = \frac{Q}{e\sqrt{\pi \cdot t'}} \quad (2.2)$$

Now using this relation in the absolute temperature contrast equation 2.3 we get,

$$\Delta T_{DAC} = T_d(t) - \sqrt{\frac{t'}{t}} \cdot T(t') \quad (2.3)$$

The actual infrared sequences information may vary from the results provided by the above equation for later times, but the DAC technique is effective in removing the non-uniform heating of the sample and improving the contrast of the image sequences after processing. A modified DAC technique using Laplace inverse transform equation 2.4 has been proposed by the author in literature [5, 11] to obtain better results for later times in comparison with actual DAC technique.

$$\Delta T_{DAC,mod}(t) = T_d(t) - \frac{\left[ l^{-1} \left[ \coth \sqrt{\frac{pL^2}{\alpha}} \right] \right]_t}{\left[ l^{-1} \left[ \coth \sqrt{\frac{pL^2}{\alpha}} \right] \right]_{t'}} \cdot T(t') \quad (2.4)$$

### Thermographic Signal Reconstruction:

The Thermal Signal Reconstruction technique also well known as TSR is the post-processing tool used to reduce high frequency temporal noise and amount of data to be manipulated while increasing the spatial and temporal resolution of thermal sequence. TSR is based on the assumption that temperature profiles for non-defective pixels follow the decay curve given by the 1D solution of the Fourier equation. The 1D solution of the Fourier equation is given by equation 2.5:

$$T(0, t) = T_0 - \frac{Q}{e\sqrt{\pi t}} \quad (2.5)$$

where  $T_0$  is the initial temperature,  $e = \sqrt{k\rho C_p}$  is the effusivity,  $Q$  is the energy absorbed by the surface in  $J/m^2$ ,  $k$  is the thermal conductivity of the material in (W/mK),  $\rho$  is the density of the material in  $Kg/m^3$  and  $C_p$  is the specific heat of the material at constant pressure in J/kgK. The 1D solution of the Fourier equation in the logarithmic form can be rewritten as in equation 2.6:

$$\ln(\Delta T) = \ln\left(\frac{Q}{e}\right) - \frac{1}{2}\ln(\pi t) \quad (2.6)$$

The 1D solution of Fourier equation in the logarithmic form is only an approximation of the Fourier transform and can be expanded using n-degree polynomial of the form:

$$\ln(\Delta T) = a_0 + a_1 \ln t + a_2 \ln^2(t) + \dots + a_n \ln^n(t) \quad (2.7)$$

The n value for the above logarithmic equation is varied between 4 or 5 to have closeness between the acquired thermal sequence and the fitted values. The fitted values are

calculated so that the noise present in the thermal sequence is reduced and thereby increasing the signal strength of the image sequences.

A synthetic thermogram sequence can be constructed using the coefficients of the logarithmic polynomial equation constructed. For each n-degree polynomial we have n+1 coefficient images from which a thermogram sequence can be reconstructed [5, 11]. The n+1 and the n coefficient images represent the background noise captured by the thermal camera. The remaining coefficient images help us develop a thermal image sequence free of noise. The synthetic data processing help reduce noise levels in the image signal, analytical processing and data compression of the images [5, 11]. The first and second time derivatives of the synthetic data coefficients generate the rate of cooling and rate of change in the rate of cooling of the inspected sample.

### **Pulse Phase Thermography:**

Pulse Phase Thermography or PPT is a processing routine that combines the advantages of Pulse Thermography (PT) and Modulated Thermography (MT) leaving behind the drawbacks of each of these techniques [16]. The PPT technique being less sensitive to the optical and infrared properties of the material generate better defect shape resolution, can reach better depths of the sample and specimens with high thermal conductivity. The technique also gives us advantage of detecting the defects in the specimens without knowing the position of the defect of sample before inspection.

In Pulse Thermography (PT) the sample is heated using a pulse heat for duration varying from  $\mu\text{s}$ , ms to s depending on the nature of the test specimen. The thermal behavior of the sample is recorded using a thermal camera. The thermal propagation equation used in the PT is  $t^2 \sim \frac{z^2}{\alpha}$ , where t is the thermal propagation time, z is the depth



of the defect and  $\alpha$  is the thermal diffusivity of the material and  $\alpha = \frac{K}{\rho C}$ , where K is thermal conductivity,  $\rho$  is density of the material and C is the specific heat. The PT technique requires prior knowledge about the captured image for contrast calculations. The contrast C of the captured images is calculated using the equation 2.8:

$$C(t) = \frac{T_i(t) - T_i(t_0)}{T_s(t) - T_s(t_0)} \quad (2.8)$$

where i and s in equation 2.8 represent the location of defective and non defective areas respectively.  $t_0$  and t represent the temperature distribution before heating and temperature distribution after heating respectively. The contrast max can be calculated at  $t_{\max}$ .

In Modulated Thermography (MT) the thermal response of the specimen generated with the help of sinusoidal temperature simulation is recorded with the help of thermal imaging camera. The sinusoidal temperature simulation period needed for the sample to be completely agitated thermally is in couple of minutes depending on the thickness and nature of the specimen. In MT the function obtained from the thermally agitated specimen is compared to a reference function. The magnitude A and phase shift  $\phi$  are computed with respect to the reference function. The magnitude A of the image represent the local optical and surface features of the sample, where as the phase shift  $\phi$  is independent of these properties but is related to propagation time delay. The MT shares same advantages as the PT, but has other drawbacks such as the speed of the acquisition of the thermal response from the specimen. The mathematical formulations of PT and MT are related to each other. In MT a single frequency is used to test the stationary

region, but in the case of PT all frequencies are simultaneously tested in the transient region.

Pulse Phase Thermography (PPT) is applied on the thermal image sequences using the Fourier transform equation 2.9,

$$F(u) = \frac{1}{N} \sum_{n=0}^{N-1} h(x) e^{-j2\pi ux} = R(u) + jI(u) \quad (2.9)$$

where  $R(u)$  and  $I(u)$  are real and imaginary components of  $F(u)$  respectively. The phase for each transformed equation is calculated using equation 2.10

$$\phi(u) = \tan^{-1} \left( \frac{I(u)}{R(u)} \right) \quad (2.10)$$

The frequencies used vary from 0 to  $\frac{1}{\Delta x}$ , where  $\Delta x$  is the time interval between the sample images. The PPT technique used for processing of the IR image sequences is less sensitive to the optical surface properties of material and has better penetration depth. The processing using PPT technique is less impact by the noises that might occur on the surface of the specimen and from the surroundings of the specimen. The acquisition time for the PPT technique is less compared to MT techniques mentioned above and can work efficiently with samples of high thermal conductivity. The PPT applied to image sequence has advantage over the PT technique as there is no need for the prior knowledge of the location or nature of the defect prior to testing of the specimen.

Once the processing technique to be used for processing the thermal image sequence is selected, the characterization of the inspected sample based on the size,

depth, and aspect ratio is to be considered. Some of the characterization methods are discussed in the following section.

### 2.3 Quantification criteria for processing

The processing tools quantify the defects of the inspected samples based on the thermal properties, size and depth of the defect with respect to non defect area. To quantify these properties of the defects, the following techniques are implemented in the processing tools.

#### **Defect Detection Algorithms:**

Many algorithms are readily available for the detection and interpretation of defects from the samples. The most common method used is manual identification [15] carried out by an experienced inspector based on the standards set by Non-Destructive Testing organizations around the world. For an automated system we use the various processing routines such as contrast, TSR and PPT discussed before.

#### **Defect Sizing:**

The defect sizing of the test sample is calculated by extracting the contour of the detected defect from the thermal sequence at peak contrast slope, at peak maximum thermal contrast or as the heating curve starts and before lateral thermal diffusion takes place between the defect and non defect area. The defect sizing is also carried out by using a proposed iterative technique [15] which is carried out by extracting the contour in each contrast image at full width half the maximum amplitude. Once the contour is extracted from each contrast image a plot of the size as a function of square root of the time is generated and the extrapolated line at time zero give us an approximate size of the defect in the sample tested.

**Data inversion and reliability:**

The data inversion computation is used to check the accuracy of each code based on the predicted size and depth of the defects. In addition to checking the robustness of the computation code, the technique also helps in accessing the processing performance of the code for different materials being inspected with various conductivity properties [16] and the effect of anisotropy.

**Code robustness:**

The code robustness for every processing tool is investigated for analyzing the behavior of the code under various experimental conditions such as the acquisition rate and duration of the capture. The processing tool capability can be computed depending on the heat distribution and surface profile of the sample and the aspect ratio of the defects in the sample.

**Ability to detect the subsurface defects, spatial resolution and depth probing:**

The detection of defect from the non defect area at a certain depth is achieved by using the contrast signal between them. The detection of the defects using contrast is carried out using two calculations [16]. Using the first method of calculation, a local signal to noise ratio is computed across the detected defects to investigate the uniformity of the thermal signal. The signal to noise ratio is calculated using the equation 2.11:

$$SNR = \frac{\sum_i^k [Pf(i)^2]}{[\sigma(N(i))]^2} \quad (2.11)$$

where  $Pf(i, j)$  is the intensity profile drawn across a defect, and noise  $N(i)$  is the difference between two profiles such as  $Pf(i)$ . The above equation used to calculate the signal to noise ratio represents the signal uniformity across the detected defects of the sample. The noise level in each thermal image sequence is calculated by calculating two

intensity profiles drawn across the defects. In the second method of calculating the contrast between the defect and non defect areas, a temperature profile is plotted across the defective and non defective areas of the sample to obtain a normalized contrast value.

#### **Comparison of various processing routines:**

In the previous reviews [16] found in thermography literature, TSR can be used as a pre-processing as well as post processing tool for thermal image sequences. The usage of TSR on thermal image sequences reduces the noise levels and enables data compression. The variations in image sequence capture such as the duration or the acquisition rate does not have much impact on the signal to noise ratio and the contrast of the processed image sequence. But the drawback of TSR is the reduction of contrast ratio between the defect and non defect area of the sample. Another drawback of the TSR technique is its inability to provide consistent depth prediction for defects of different aspect ratios at same depth.

In PPT each pixel's temperature time history is transformed into frequency domain. This frequency domain is used to generate phase and amplitude imaging. The drawback of PPT is the need to have different frequency domains to generate different defects at different depths in the test sample. From literature [16] that there is an increase in signal to noise ratio of the thermal image sequences with the increase in acquisition rate of the images.

The use of contrast processing tools such as the Dynamic thermal tomography (DTT) mentioned in the literature [16] are sensitive to heat source thermal profile. The signal to noise ratio calculated using intensity profile to different defects at various depths show similar results. The DDT technique provides similar results for thermal sequences captured at different acquisition rates and experimental durations. But the

performance of the DDT technique is affected by the isotropic, anisotropic and thermal conductivity of the sample. The signal to noise ratio of the processed anisotropic samples showed less visibility of defects due to low thermal conductivity compared to that of the same isotropic samples. It is observed from the literature that the DDT provided consistent depth prediction accuracy for same depth, different aspect ratio defects but consistency declines with change in the thermal and material properties of sample.

All the present processing techniques used for thermal image processing are applied only to the infrared image sequences of samples generated using short optical pulse and their effectiveness of processing the thermal image sequences is considerably reduced when the heating technique is changed to either steady state or electromagnetic excitation. Developing a technique that could be applied to thermal image sequences generated using different thermal excitation sources will be the next big step in thermal processing.

## Chapter 3

### **3 PRINCIPAL COMPONENT ANALYSIS**

The processing techniques discussed so far are applied to infrared image sequences obtained by using short optical pulse to heat surface of the sample. Even with the advancement in the processing tools used for processing thermal image sequences, there is no generic method to process the image sequences generated using various thermal excitation techniques to enhance the contrast between the defect and non defect areas. To facilitate the processing of the infrared image sequences generated using different heating techniques we use the statistical analysis tool Principal Component Analysis.

Principal Component Analysis (PCA) is a statistical analysis tool used for identifying patterns in data and expressing the data in way to highlight the similarities and differences in the patterns. The pattern matching of the data becomes very difficult when the data dimension is very high. In such situations PCA comes in handy for analyzing and graphically representing of such data. Once the patterns in the data are found, the data is compressed by reducing the data dimensions without much loss of information.

#### 3.1 Literature Survey on Principal Component Analysis

PCA is very old method developed in the year 1901 by Pearson, but its prominence was brought out by Hotelling in 1933. PCA is a classical technique which can be applied for applications in linear domain such as signal processing, image processing, system and control theory and communications where a huge lump of data is to be analyzed. PCA is used in a wide areas where data compression and pattern

matching is of high priority. Some of fields where PCA is applied for data compression carried and better pattern matching is carried out are discussed in the following sections.

### **Singular Value Decomposition (SVD) and Principal Component Analysis (PCA) for gene expression data:**

Michael E.W [17] described that PCA/SVD is the well suited statistical analysis techniques for the multivariate data such as the gene expression data. The SVD is used in comparison to actual PCT as large amount of data is captured, such as tens of hundreds of data points from a single microarray experiment. The generated gene data from the microarray experiments is highly noisy, so a technique is to be developed that could detect, visualize and gather important information from such data. The use of SVD seems to be apt for this application as it can aid in detecting biologically meaningful signals from the generated data. The SVD used for gene expression data helps us resolve gene groups and detect underlying gene expression patterns. With the application of SVD on the obtained experimental data, the gene groups can be classified using transcriptional response. The first and second singular vectors obtained from the SVD consist of most of the meaningful information of the obtained biological data. The SVD data analysis carried out on gene data showed that the technique is unique and works well when there is a complicated distribution of gene data in the experimental data. The presence of weak patterns in the experimental data and the structure of data do not allow separation of data points, causing clustering algorithms to fail. The biologically meaningful patterns are detectable using this technique, where the other commonly used procedures fail for this application.



## **Principal component thermography for flaw contrast enhancement and flaw depth characterization in composite structures:**

Rajic N [18, 19] has proposed the use of principal component thermography technique to process the IR image sequences obtained from testing composite structures to enhance the contrast of acquired images. The proposed technique is applied on flash thermographic inspection data of the composite structures. The Principal component analysis (PCA) applied on thermographic image data is called as Principal Component Thermography (PCT). The proposed PCT is a statistical analysis tool applied to multivariate data. The method helps to reduce the unwanted noise levels present in the captured image sequences and increase the contrast of the processed images compared to unprocessed data. In some previous techniques such as PPT, the duration of heating and nature of the material are the key entities to be known for processing the thermographic image data. In PPT we need to rely on a set of prescribed basis functions which is not the case in PCT. We use a set of orthogonal statistical modes to enhance the contrast of the captured thermal images. The SVD base PCA is used to actual PCT due to the volume of image data captured in a single thermographic experiment. In the SVD based PCT the IR sequences are subject to preprocessing to normalize the data to reduce the effects caused by reflection and disturbances from surroundings. Once the normalization is completed we apply the PCT on the data and the first empirical orthogonal function is plotted to obtain the enhanced image. In PCT the first two or three empirical orthogonal functions contain nearly 90 percent of the variability of the image data and the remaining variability is present in the corresponding functions which can be neglected due to huge computation requirements. The proposed method has produced better contrast processed

images compared to the other available processing routines such as PPT and image averaging.

### **Statistical Analysis of IR thermographic sequences by PCT:**

In the Statistical analysis of IR thermographic sequences by PCT provided by S. Marinetti [20], thermal imaging cameras are used to capture the infrared image sequences from the test sample. The image data captured by the IR cameras consist of undesirable signals and noise along with the IR image data. These image sequences are to be processed to eliminate the undesirable signals and enhance the useful IR information. The PCT is applied on the sequence of images to extract features and reduce undesirable signals by projecting original data onto a system of orthogonal components. The PCT used for processing IR sequences is mainly based on thermal contrast evaluation in time. The spatial evaluation of the IR sequences is rarely used. The PCT analysis is mainly based on the second order statistics of IR image data. The processing of the IR images provides us with good results, but is very difficult to predict the processed results. This drawback of PCT processing prevents us from using it in automated systems.

The SVD computation technique is used in place of actual PCT to reduce the amount of computation that is needed. The use of SVD helps to increase the computation speed and the hardware requirements needed to do large computations as in the PCT. The results obtained from SVD have the same dimension as the inputted image used for processing. In this technique a matrix called scatter matrix is created on which the SVD is applied. The scatter matrix is a matrix of lower dimension which is obtained by projecting the original image sequence matrix into a new set of principal axis. Two processing techniques are applied on scatter matrix for processing using the PCT. The

first one is to subtract the mean image from each image to reduce the uneven heating and absorption distribution of the sample. The second image is chosen instead of the first image available after the flash, so that we can reduce the effect of reflection coming from the heat source. The second technique is to subtract the mean temporal profile instead of the mean image. Once the processing is done, the temporal and spatial profiles are plotted. The first three components show the maximum variance of the data. In both the cases the SNR are proved to be similar. The variance is now 68% compared to 95% in the first technique. The samples used for the experiment are steel plates with 6 circular bottom holes, opaque plastic with nine square shaped bottom holes.

In the following sections PCT and SVD based PCT methodologies are discussed with their application to thermography technique.

### 3.2 Principal Component Analysis Method

In PCA the data is projected from its original space to its eigenspace to increase the variance and reduce the covariance so as to identify patterns in data. The algorithm as shown in figure 3.2.1 is followed to apply Principal Components Analysis on a data set. In the PCA the first step is to collect the data set to be analyzed. The mean value for the data set is calculated. The calculated mean value is subtracted from the data set to normalize the data. The covariance matrix is calculated for the normalized data matrix. From the covariance matrix we calculate the eigenvalues and the corresponding eigenvectors. The eigenvectors are arranged in the descending order of magnitude in the eigenvector matrix. The eigenvector with the highest eigenvalue is the principal component of the data set. In most cases more than 95% of variance is contained in the

first three to five components. Using the principal components we rebuild the data which highlighting the similarities and dissimilarities.

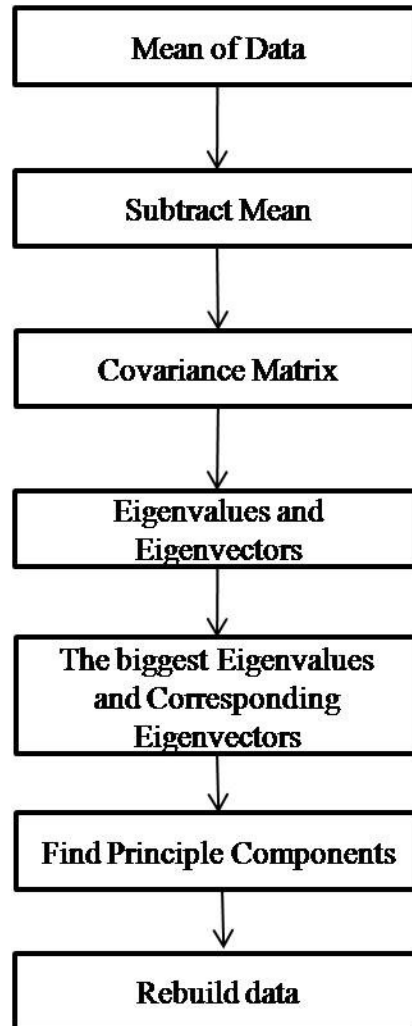


Figure 3.2.1: Flow diagram of PCT

### 3.3 PCT for Thermal Image Sequence

The Principal Component Analysis applied to thermography is known as Principal Component Thermography (PCT). The image sequence containing the information about the sample is captured using a thermal imaging camera. The thermal image sequence is similar to the sequence of images shown in figure 3.3.1. The thermal image sequence is a

3D image matrix consisting of  $N_t$  number of image frames with each image frame consists of  $N_x$  horizontal elements and  $N_y$  vertical elements. To apply PCT on the thermal image sequence a matrix operation discussed below is applied to convert the 3D image matrix into a 2D image matrix.

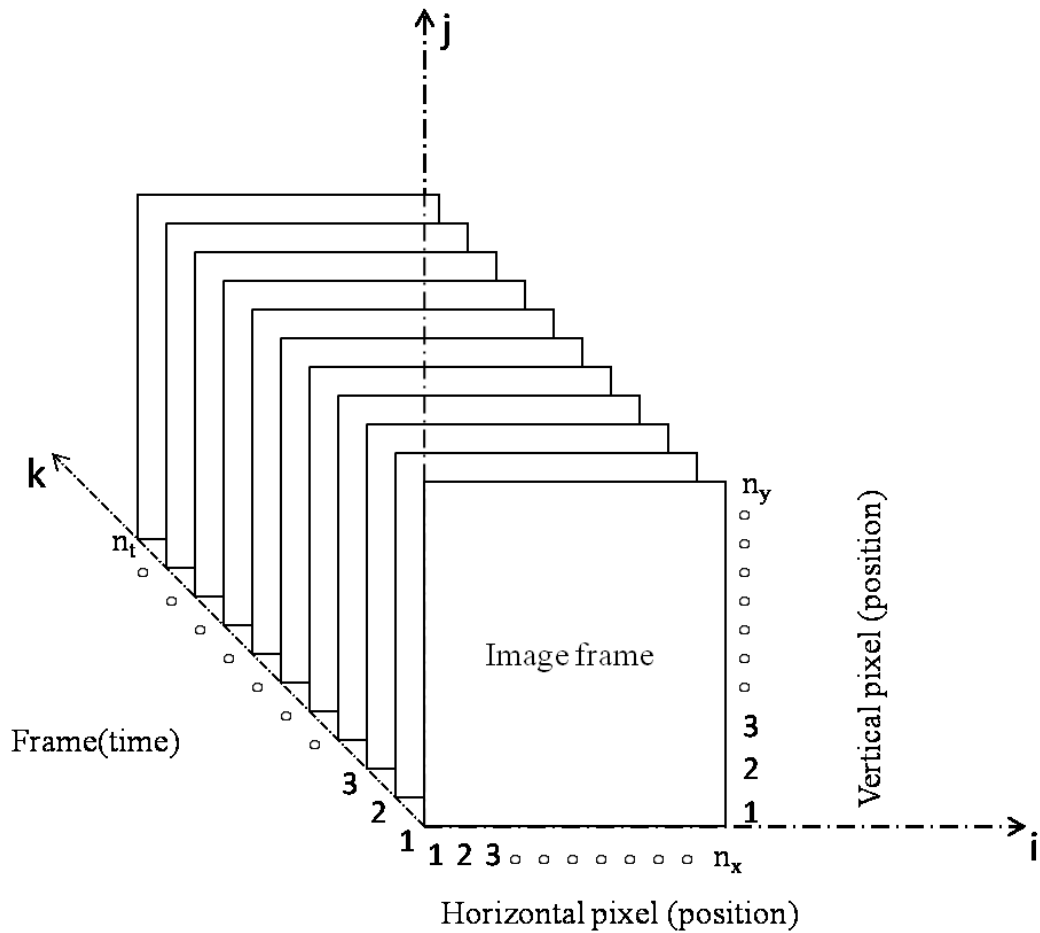


Figure 3.3.1: Sequence of  $N_t$  image frames each with  $N_x$  and  $N_y$  elements

**Constructing Raster like Matrix:** Each image frame of size  $N_x$  by  $N_y$  can be represented as an  $N_x N_y$  dimensional vector  $X$ ,

$$X = (x_1 \ x_2 \ x_3 \ \dots \ x_{N_x N_y})$$

where the rows of pixels in the image are placed one after the other to form a one dimensional image. The first  $N_x$  elements in the dimensional vector will be the first row of the image, the next  $N_x$  elements are the next row of the image and so on. The values in the vector are the intensity values of the image. Similarly we do the same for all the  $N_t$  images in the captured image sequence. The 2D image matrix is generated with each row containing the information about each frame of the image sequence and the column containing the  $N_t$  number of image vectors. This matrix is also known as raster-like matrix. Once we have the 2D matrix we follow the algorithm of PCT as shown in Figure 3.2.1.

Once we have the 2D matrix of the infrared image sequence, the mean of the data is calculated. The calculated mean value is subtracted from the data set to normalize the data. The normalized data is used to calculate the covariance matrix. The covariance matrix can be calculated using equation 3.1.

$$C = \frac{1}{N}XX^T \quad (3.1)$$

where  $X$  is the matrix obtained after normalization and  $C$  is the covariance matrix. Since the data is  $N_xN_y$  dimensional, we get the covariance matrix of size  $N_xN_y \times N_xN_y$  dimension. The eigenvalues and eigenvectors can be found using matrix diagonalization according to equation 3.2.

$$C_D = P^{-1}CP \quad (3.2)$$

where  $C$  is the covariance matrix,  $C_D$  is the diagonalized matrix with eigenvalues on the diagonal,  $P$  is the matrix with eigenvectors as its columns. Since the data is  $N_xN_y$  dimensional we get  $(N_xN_y \times N_xN_y)$  dimension covariance matrix and  $N_xN_y$  eigenvectors. The matrix  $C_D$  is reordered to make the eigenvalues in a descending order and also

reorder the matrix  $P$  in the similar order. To reduce the dimension of the original matrix, reserve the first  $K$  columns in matrix  $P$  to form matrix  $P_K$ . The original matrix is converted to the new basis using equation 3.3.

$$C_P = P_K^T C \quad (3.3)$$

The result image is reconstructed using the dimensionally reduced raster-like matrix  $C_P$ .

The choice of  $K$  is based on the desired amount of the variance proportion retained in the first  $K$  eigenvalues according to equation 3.4.

$$r = \frac{\sum_{i=1}^K e_i}{\sum_{i=1}^M e_i} \quad (3.4)$$

where  $e_i$  is the  $i$ th eigenvalue of the diagonal matrix  $C_D$ . In most cases more than 95% of variance is contained in the first three to five principal components.

**Limitations of PCT:**

- a. The PCT processing of infrared image sequences can be used when the raster matrix size is limited to  $10^4$ .
- b. The size of covariance matrix becomes very huge when the raster matrix size exceeds  $10^4$ .
- c. The calculation of the diagonal matrix and eigenvalues for the 2D matrix is computation intense.
- d. The hardware requirement for processing such data very high.

To overcome the problem of huge matrix computation, we need to use a technique which does the same operation but with less computation requirements and ease of processing the input data. So Singular Value Decomposition (SVD) based PCT is used to overcome the limitations of the PCT. The computation procedure of SVD based PCT is described in the following section.

### 3.4 Singular Value Decomposition (SVD) based PCT Method

The SVD based PCT is applied on the data set following the algorithm as shown in figure 3.4.1. In the SVD based PCT the first step is to acquire the data set to be analyzed. The mean value for the data set is calculated. The calculated mean value is subtracted from the data set to normalize the data. Once the data is normalized we apply the SVD on the data using equation 3.5 to calculate the decomposed matrices  $U$ ,  $S$  and  $V$  to obtain the principal components. The decomposed matrix  $U$  consists of empirical orthogonal functions that represent the spatial variation of the data set. Each column of  $U$  gives the coordinates of data set in the space of principal components. The matrix  $S$  is diagonal matrix with singular values on its diagonal. The singular values in the matrix  $S$  are the eigenvalues for the corresponding eigenvectors in the matrix  $V$ . The eigenvalues in  $S$  are reordered to arrange them in descending order of their value. The columns of matrix  $V$  or the rows of matrix  $V^T$  are the principal components or eigenvectors of the data set which are sorted in the descending order of magnitude. The first few columns of matrix  $U$  are used to reconstruct the data to reduce the redundancy in the original data set.

### 3.5 Singular Value Decomposition (SVD) for Thermal Image Sequence

The thermal image sequence containing the information about the sample is processed using SVD based PCT. The 3D image matrix is converted to 2D matrix using the similar method as described in actual PCA to build the raster like matrix  $A$ . The raster matrix  $A$  consists of  $N_t$  as matrix rows,  $N_x N_y$  as matrix columns as shown in figure 3.5.1. Once we have the raster like matrix  $A$ , the mean from each data point is subtracted to create zero-centered data. Each column of the raster matrix has all pixel values of an image frame. The mean image is the mean of the values of each column. Once the zero



centered data is calculated, the SVD transformation is applied to find the eigenvalues and eigenvectors using equation 3.5.

$$A = USV^T \quad (3.5)$$

Once we obtain the three matrices  $U$ ,  $S$  and  $V^T$ , using the first few columns of matrix  $U$  which are the empirical orthogonal functions give the coordinates of matrix  $A$  in the space of principal components. The resulting image constructed using the empirical orthogonal functions from matrix  $U$  shows good contrast difference between the defect and non defect area along with reducing the redundant data from the original matrix  $A$ .

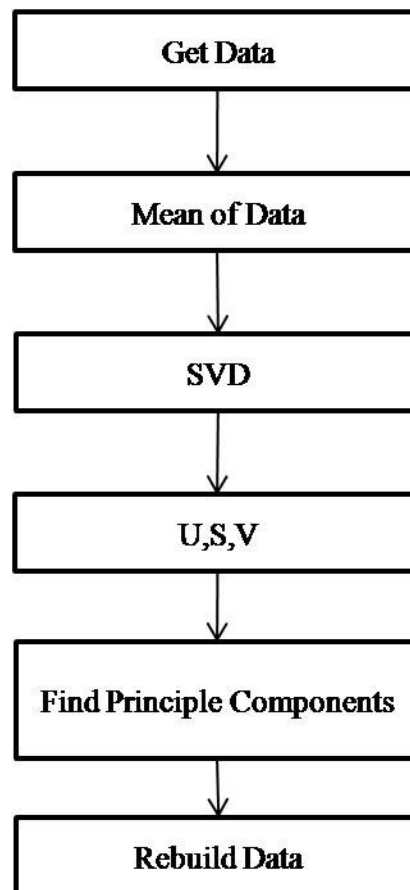


Figure 3.4.1: Flow diagram of SVD based PCT

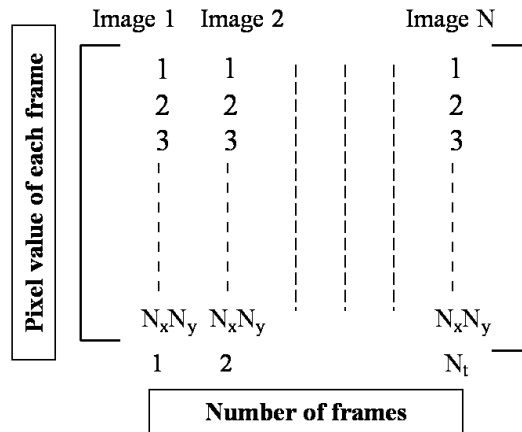


Figure 3.5.1: 2D raster matrix with image sequence

Though SVD based PCT is an efficient way of PCT when we have very high data volume, we still have the problem of processing image sequences of large samples. To overcome this problem a new technique called as economical SVD is proposed which can process data in a more efficient way. Economical SVD is discussed in more detail in the next chapter.

## Chapter 4

### **4 ECONOMICAL SINGULAR VALUE DECOMPOSITION TECHNIQUE**

The proposed Economical Singular Value Decomposition technique reduces the computation time needed to analyze the thermographic data along with better contrast ratio between the defect and non defect area. The algorithm shown in figure 4.1.1 followed for Economical SVD based PCT. The first step in the Economical SVD based PCT is to acquire the data set to be analyzed. A normalization operation is applied on the acquired data set to reduce the side effects caused by uneven heating and noises from surrounding environment to create a zero centered data in each dimension.

The economical SVD is applied on the normalized data using equation 4.4 to calculate the matrices  $U$ ,  $S$  and  $V$  to get the principal components. The decomposed matrix  $U$  consists of empirical orthogonal functions that represent the spatial variation of the data set. Each column of  $U$  gives the coordinates of data set in the space of principal components. In the Economical SVD we calculate the columns in matrix  $U$  equal to the number to number of image frames we process from the thermal image sequence to reduce the amount of processing needed on thermal image. The matrix  $S$  is diagonal matrix with singular values on its diagonal. The singular values in the matrix  $S$  are the eigenvalues for the corresponding eigenvectors in the matrix  $V$ . The eigenvalues in  $S$  are reordered to arrange them in descending order of their value. The columns of matrix  $V$  or the rows of matrix  $V^T$  are the principal components or eigenvectors of the data set which are sorted in the descending order of magnitude. The first few columns of matrix  $U$  are used to reconstruct the data to reduce the redundancy in the original data set.

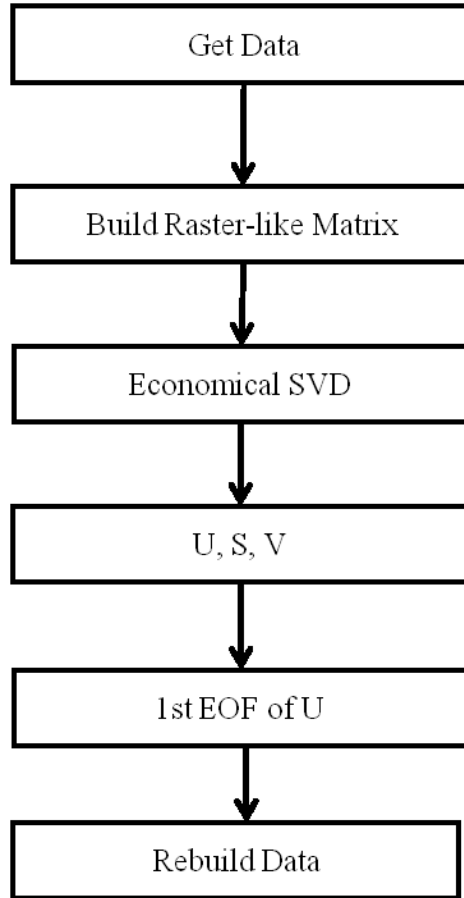


Figure 4.1.1: Flow diagram of Economical SVD

#### 4.1 Economical Singular Value Decomposition (SVD) for Thermal Image Sequence

The thermal image sequence containing the information about the sample is captured using a thermal imaging camera. The thermal image sequence is similar to the sequence of images shown in figure 4.1.2. The thermal image sequence is a 3D image matrix consisting of  $N_t$  number of image frames with each image frame consists of  $N_x$  horizontal elements and  $N_y$  vertical elements. To apply Economical SVD based PCT on the thermal image sequence a matrix operation is needed to convert the 3D image matrix into a 2D image matrix.

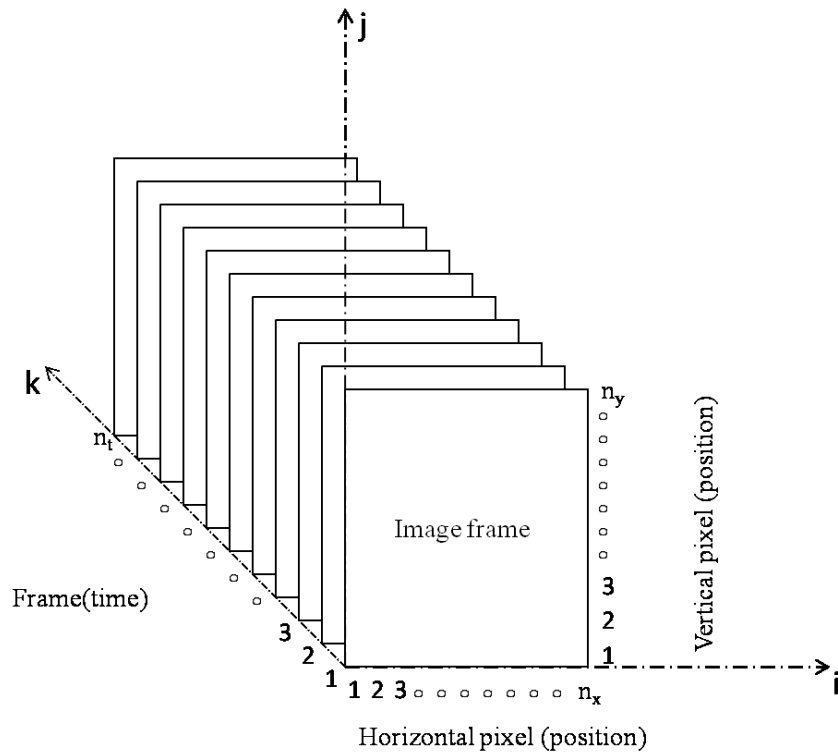


Figure 4.1.2: Sequence of  $N_t$  image frames each with  $N_x$  and  $N_y$  elements

**Constructing Raster like Matrix:** Each image frame of size  $N_x$  by  $N_y$  can be represented as a as an  $N_x N_y$  dimensional vector,

$$X = (x_1 \ x_2 \ x_3 \ \dots \ \dots \ x_{N_x N_y})$$

where the rows of pixels in the image are placed one after the other to form a one dimensional image. The first  $N_x$  elements in the dimensional vector will be the first row of the image, the next  $N_x$  elements of the dimensional vector are the next row of the image and so on. The values in the vector are the intensity values of the image. Similar procedure is followed to convert all the  $N_t$  images in the captured image sequence into dimensional vectors. There two ways in which the dimensional vectors can be arranged in the matrix  $A$ . The first method is to arrange the dimensional vectors row wise in the

matrix  $A$  i.e. to have  $N_x N_y$  number of columns and  $N_t$  number of rows as shown in figure 4.1.3. The second method is to arrange the dimensional vectors column wise in the matrix  $A$  i.e. to have  $N_x N_y$  number of rows and  $N_t$  number of columns as shown in figure 4.1.4. Physically, these two 2D matrices have different meanings. The first One uses the mean temporal profile to remove temporal constant and the second one uses the mean image to remove spatial constant. However, mathematically, these two 2D matrices are interchangeable through a matrix transpose operation and subtraction off the mean of each row or the mean of each column. In the economical SVD based PCT, the second case is selected.

The normalization operation on the matrix  $A$  can be carried out in two ways. In the first case we use the mean of the image and in the second case we normalize the matrix  $A$  using equations 4.1, 4.2 and 4.3 as mentioned in the literature [19] to form the matrix  $\hat{A}$ . In the current approach we use the mean image of the image frame to normalize the image sequence to reduce the side effects caused by uneven heating and noises and create a zero centered data in each dimension.

$$\hat{A}(m, n) = \frac{A(m, n) - \mu_n}{\sigma_n} \quad (4.1)$$

$$\mu_n = \frac{1}{M} \sum_{m=1}^M A(m, n) \quad (4.2)$$

$$\sigma_n = \sqrt{\frac{1}{M-1} \sum_{m=1}^M (A(m, n) - \mu_n)^2} \quad (4.3)$$

Once the normalization of the data matrix is completed, the economical SVD transformation is applied on the normalized matrix  $\hat{A}$  using equation 4.4 to get the empirical orthogonal functions. The decomposed matrix  $U$  consists of empirical

orthogonal functions equal to the number of  $N_t$  images in the image sequence. The empirical orthogonal functions of matrix  $U$  represent the spatial variation of the defect of the test sample. The first and second columns of the matrix  $U$  are the first and second empirical orthogonal functions represent nearly 80 to 90 percent of the variation of the data collected. The matrix  $S$  is a diagonal matrix with singular values on its diagonal arranged in the descending of their magnitude. The columns of matrix  $V$  represent the principal components or the direction of the defect of the sample. Finally, the result spatial image is rebuild by using the first empirical orthogonal function from the matrix  $U$ .

$$\hat{A} = USV^T \quad (4.4)$$

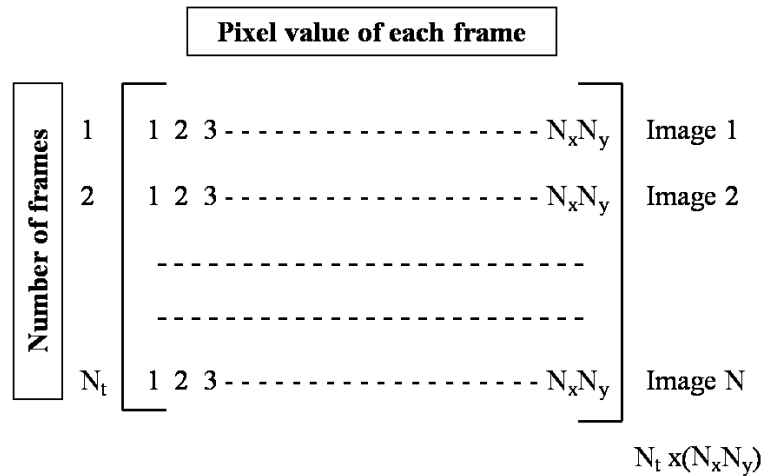


Figure 4.1.3: 2D raster matrix with  $N_t$  rows and  $N_x N_y$  columns

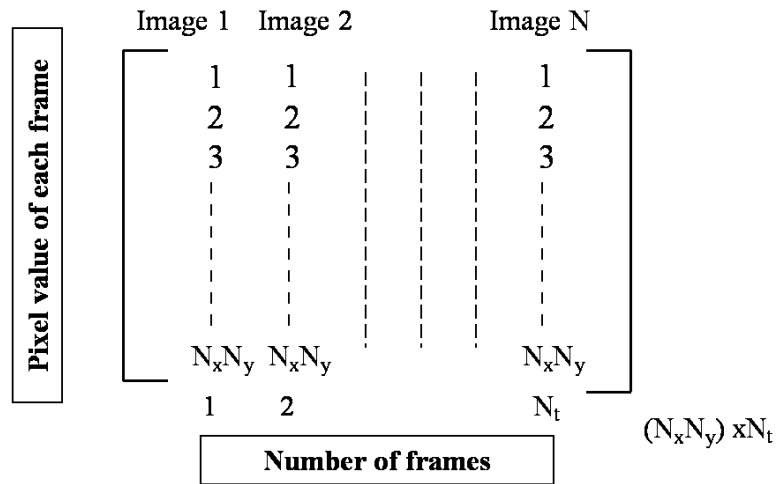


Figure 4.1.4: 2D raster matrix with  $N_x N_y$  rows and  $N_t$  columns



## Chapter 5

### 5 LABORATORY TESTS

In this chapter thermography experiments conducted using different thermal excitation sources such as pulse, halogen and induction are discussed and the results obtained by applying the proposed economical SVD based PCT processing routine on the captured thermal image sequences are compared with the available processing routines such as the SVD and TSR.

#### 5.1 Test Specimen

Test sample used for the thermography experiment is galvanized (GA) steel panels with three circular adhesive spots of different dimensions between them, similar to the hem joints in the automotive industry. The surface finish of the specimen being highly reflective is painted using black emissivity paint of emissivity 0.94 to reduce the effects of reflection. The sample used for the inspection is shown in figure 5.1.1 and figure 5.1.2 and the sample specifications are as shown in tables 5-A and 5-B



Figure 5.1.1: Test Sample black painted



Figure 5.1.2: Test Sample unpainted

Adhesive Spots	Diameter(mm)
Spot 1	9.144
Spot 2	18.5166
Spot 3	26.9875

	Thickness(mm)
Panel 1	0.6858
Panel 2	0.6835
Adhesive Spots	0.2794

Table 5-A: Adhesive spot dimensions

Table 5-B: Sample Dimensions

## 5.2 Thermal Cameras

Two thermal imaging cameras, i) FLIR Thermovison A40M uncooled infrared camera ii) FLIR Phoenix DTS cooled infrared camera are used to capture the thermal image sequences from the specimen. The specifications of the cameras are given in table 5-C.



Camera Specifications		
Description	Cooled camera	Uncooled camera
<b>Model Name</b>	FLIR Phoenix DTS	FLIRA40M
<b>Camera Images</b>		
<b>Resolution of the Camera</b>	640x512	320x240
<b>Focal Plane Array Cooling(FPA)</b>	74°K	No Cooling
<b>Sensitivity(NETD)</b>	0.025K	0.08K
<b>Frame Rate</b>	Changes with Integration time and Resolution	7.5 Hz, 15 Hz, 30 Hz and 60 Hz

Table 5-C: Thermal Cameras Specifications

### 5.3 Heat Sources

The heat sources used to thermally excite the samples include Halogen, Flash and Induction. The specifications of the heat sources used are discussed in the following sections.

**Halogen Heating:** The test specimen is thermally excited by steady state heating for a specific period of time using halogen lamps. The halogen heating source comprises of eight halogen lamps each giving out 500watts of heat to the test sample. After the sample being heated using the halogen lamps for a specific period of time, the heat source is covered using shutters to avoid the residual heat for the lamps exposing on the sample. The entire heating and the cooling curve of the sample is recorded using the thermal imaging cameras. The specifications of the halogen lamps are given in table 5-D and the heat source shown in figure 5.3.1.

Heat Source - Halogen	
Manufacturer	Custom Made
Number of Lamps	8
Power of Each Lamp	500w
Total Power from the system	4000w



Table 5-D: Halogen Specifications

Figure 5.3.1: Halogen Heating Source

**Pulse\Flash Heating:** In flash heating, a short heat pulse that lasts for a few seconds to thermally excite the test sample. The flash heat source is built using four flash lamps that give out total heat output of 6000watt per second. The entire heating and the cooling

curve of the sample is recorded using the thermal imaging cameras. The specifications of the flash lamps are given in table 5-E and the heat source shown in figure 5.3.2.

Heat Source - Flash	
<b>Manufacturer</b>	Power Pack -Bowens Flash Lamps-Caulmet
<b>Model Name</b>	Quadx 3000
<b>Maximum Power Output</b>	2x3000w/s
<b>Minimum Power Output</b>	31w/s

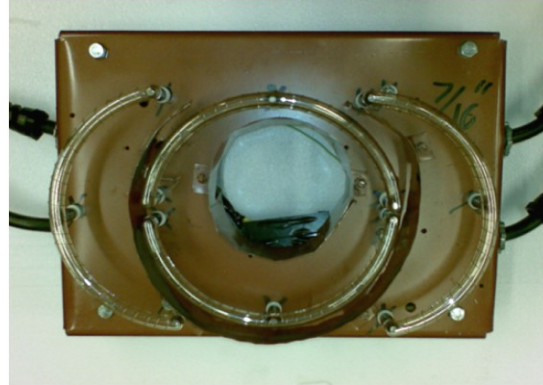


Table 5-E: Flash Specifications

Figure 5.3.2: Flash Heating Source

**Induction Heating:** In induction heating of the test sample, a magnetic field is induced based on the equation 5.1 into the sample which thermally excites the defect and non defect area based on their induction properties. The difference in the induction properties heats the defect and non defect areas to different thermal variations. These thermal variations are recorded using the thermal imaging cameras. The induction heat source gives out 1000watts of heat on to the sample. The entire heating and the cooling curve of the sample is recorded using the thermal imaging cameras. The specifications of the induction heater are given in table 5-F and the heat source and coils used in the heater are shown in figure 5.3.3, 5.3.4 and 5.3.5 respectively.

$$\epsilon = -\frac{d\phi}{dt} \quad (5.1)$$

where  $\epsilon$  is the electromotive force (emf) in volts and  $\phi$  is magnetic flux in webers.

Heat Source - Induction	
Manufacturer	Induction Heater and Coils - Ameritherm Inc
Model Name	Hotshot
Current Output	(0-300)amps

Table 5-F: Induction Specifications



Figure 5.3.3: Induction Heating Source

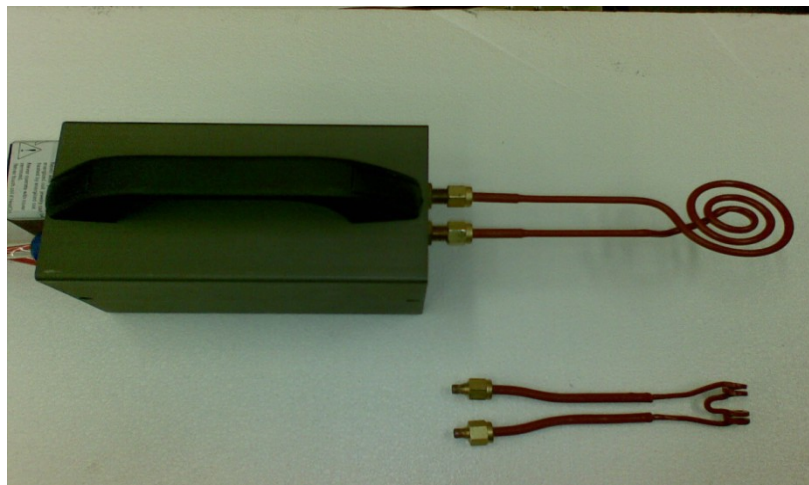


Figure 5.3.4: Various induction coils

### Induction Coil



Diameter of the induction coil - 6 cm

Diameter of coil used to make induction coil - 5mm

Maximum area can be heated – 6cm

Figure 5.3.5: Induction coil specifications

### 5.4 Thermography using Flash as Heat Source

The test sample is thermally excited using the flash lamps in the experimental setup as shown in the figure 5.4.1. The thermal image sequence of the test sample is

captured using the thermal imaging camera shown in figure 5.4.1. The captured thermal image sequence is processed using the PCT SVD, Economical SVD and TSR processing routines and the results compared. In all the three processing routines, the thermal image sequences are loaded into their respective programs and Region of Interest (ROI) of the thermal image sequence to be processed is selected. Once the ROI of the thermal image sequence is selected, the processing routines carry out their respective processing techniques to enhance the contrast between the defect and non defect area of the sample.

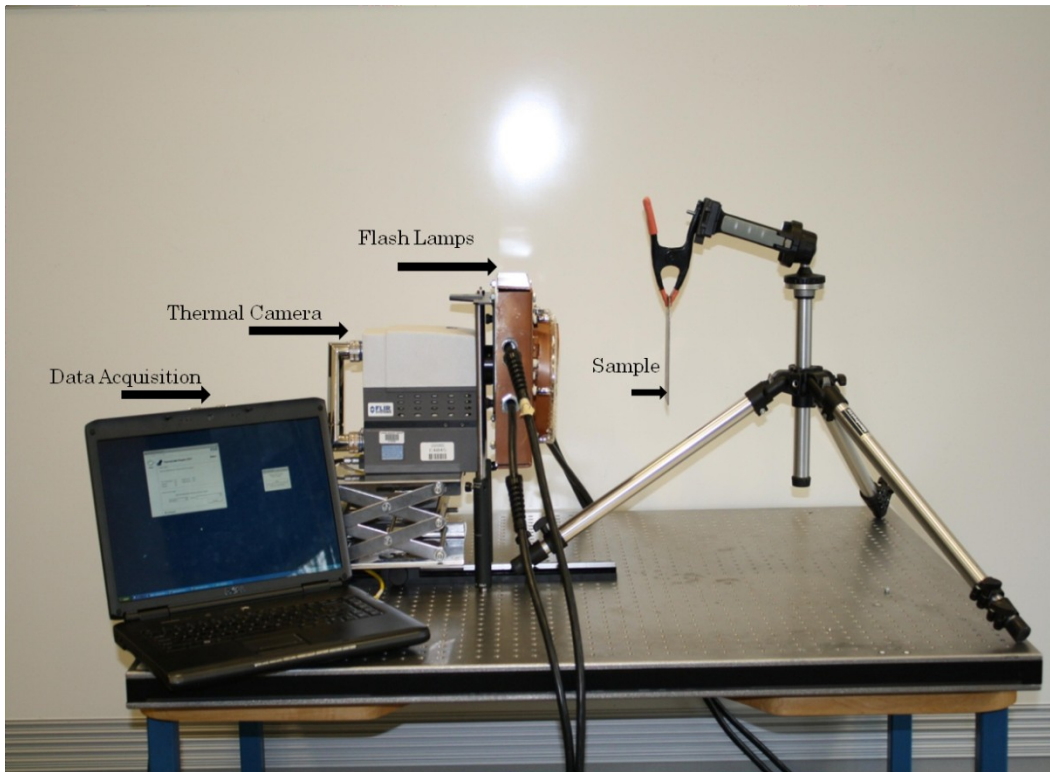


Figure 5.4.1: Flash Heating Source Experiment

**Economical SVD PCT:** In the Economical SVD based processing technique the thermal image sequence is loaded in to program and the region with all the three adhesive spots is selected as region of interest as shown in figure 5.4.2a. The processing routine processes

the raw image as shown in figure 5.4.2b and the processed image shown in figure 5.4.2c is generated with higher contrast and edge visibility compared to the raw image.

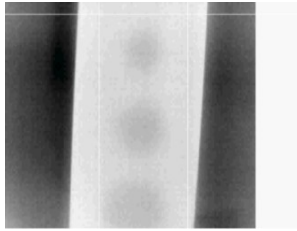


Figure 5.4.2(a)



Figure 5.4.2(b)

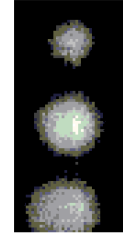


Figure 5.4.2(c)

Figure 5.4.2: Economical SVD based PCT Processing and Results of test sample using Flash Heat Source. Figure 5.4.2(a): ROI of Economical SVD based PCT. Figure 5.4.2(b): Raw image before processing using Economical SVD based PCT. Figure 5.4.2(c): Result image of Economical SVD based Processing.

*Profile Intensity Calculation:* The intensity between the defect and non defect area of the sample is calculated by drawing a line profile from one end of the ROI to the other end as shown in the figure 5.4.3(a). The calculated intensity is plotted along the distance of the profile of sample as shown in the figure 5.4.3(b). Similar to the raw image, the line profile of the processed image is drawn as shown in the figure 5.4.3(c) and the calculated intensity for the line profile is plotted as shown in figure 5.4.3(d). The intensity variation observed in the processed image is much higher than that of the raw image.

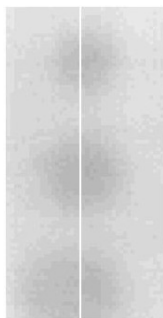


Figure 5.4.3(a)

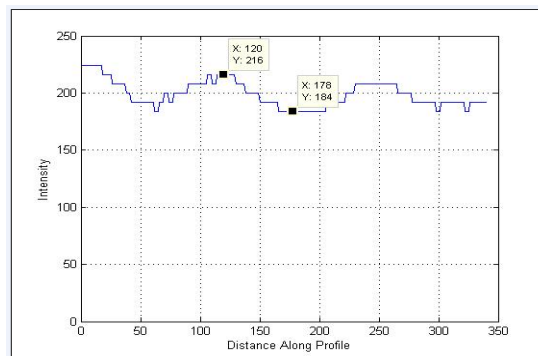


Figure 5.4.3(b)

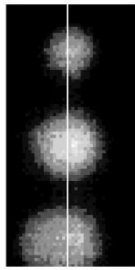


Figure 5.4.3(c)

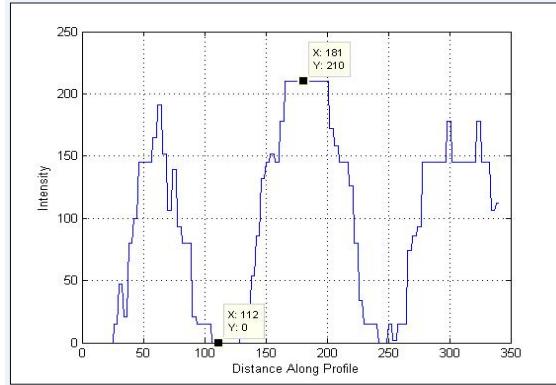


Figure 5.4.3(d)

Figure 5.4.3(a): Raw image with line profile before processing. Figure 5.4.3(b): Raw image intensity profile before processing using Economical SVD based PCT. Figure 5.4.3(c): Result image with line profile after Economical SVD based PCT processing. Figure 5.4.3(d): Result image intensity profile after processing using Economical SVD based PCT processing.

**SVD based PCT:** In the SVD based processing technique the thermal image sequence is loaded in to program and the region with least size adhesive spot is selected as region of interest as shown in figure 5.4.4(a) due to processing limitations of the routine. The processing routine processes the raw image as shown in figure 5.4.4(b) and the processed image shown in figure 5.4.4(c) is generated with higher contrast and edge visibility compared to the raw image.

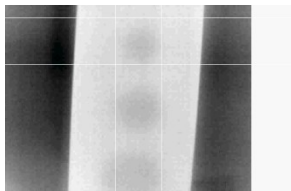


Figure 5.4.4(a)



Figure 5.4.4(b)



Figure 5.4.4(c)

Figure 5.4.4: SVD based PCT Processing and Results of test sample using Flash Heat Source. Figure 5.4.4(a): ROI of SVD based PCT. Figure 5.4.4(b): Raw image before processing using SVD based PCT. Figure 5.4.4(c): Result image of SVD based Processing.



*Profile Intensity Calculation:* The intensity between the defect and non defect area of the sample is calculated by drawing a line profile from one end of the ROI to the other end as shown in the figure 5.4.5(a). The calculated intensity is plotted along the distance of the profile of sample as shown in the figure 5.4.5(b). Similar to the raw image, the line profile of the processed image is drawn as shown in the figure 5.4.5(c) and the calculated intensity for the line profile is plotted as shown in figure 5.4.5(d). The intensity variation observed in the processed image is similar to that obtained using economical SVD.

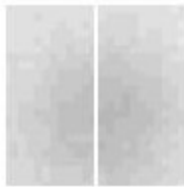


Figure 5.4.5(a)

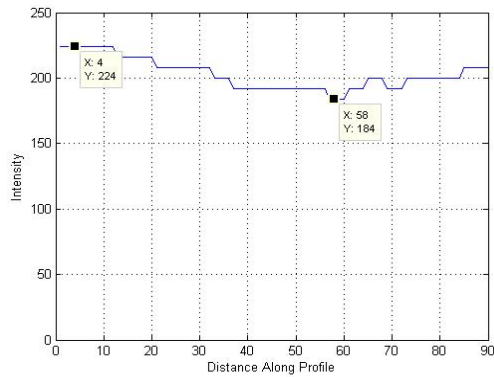


Figure 5.4.5(b)

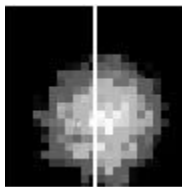


Figure 5.4.5 (c)

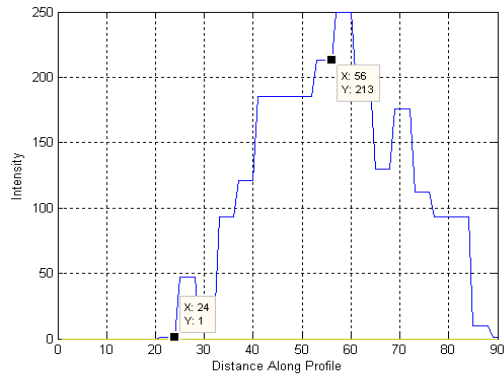


Figure 5.4.5(d)

Figure 5.4.5(a): Raw image with line profile before processing. Figure 5.4.5(b): Raw image intensity profile before processing using SVD based PCT. Figure 5.4.5(c): Result image with line profile after SVD based PCT processing. Figure 5.4.5(d): Result image intensity profile after processing using SVD based PCT processing.

**Thermal Signal Reconstruction (TSR):** In the TSR based processing technique the thermal image sequence is loaded in to program and the region with least size adhesive spot is selected as region of interest as shown in figure 5.4.6(a). The processing routine processes the raw image as shown in figure 5.4.6(b) and the processed image shown in figure 5.4.6(c) is similar in contrast caompared to the raw input image. There is no edge detectibility of the adhesive between the GA steel panels.

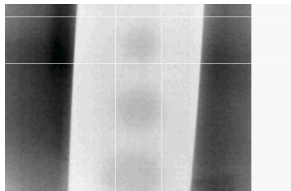


Figure 5.4.6(a)



Figure 5.4.6(b)

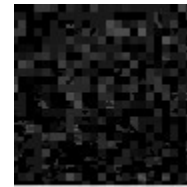


Figure 5.4.6(c)

Figure 5.4.6: TSR Processing and Results of test sample using Flash Heat Source  
Figure 5.4.6(a): ROI of TSR. Figure 5.4.6(b): Raw image before processing using TSR.  
Figure 5.4.6(c): Result image of TSR Processing.

*Profile Intensity Calculation:* The intensity between the defect and non defect area of the sample is calculated by drawing a line profile from one end of the ROI to the other end as shown in the figure 5.4.7(a). The calculated intensity is plotted along the distance of the profile of sample as shown in the figure 5.4.7(b). Similar to the raw image, the line profile of the processed image is drawn as shown in the figure 5.4.7(c) and the calculated intensity for the line profile is plotted as shown in figure 5.4.7(d). The intensity variation observed in the processed image is comparatively less than the other two techniques it is compared with.

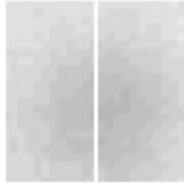


Figure 5.4.7(a)

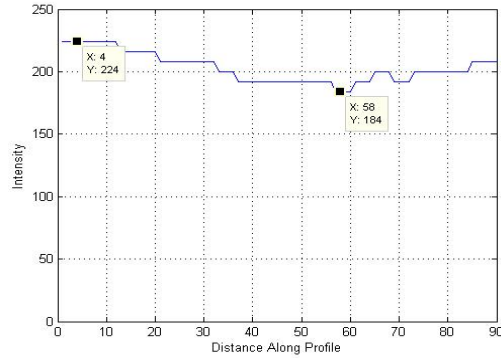


Figure 5.4.7(b)

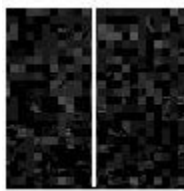


Figure 5.4.7(c)

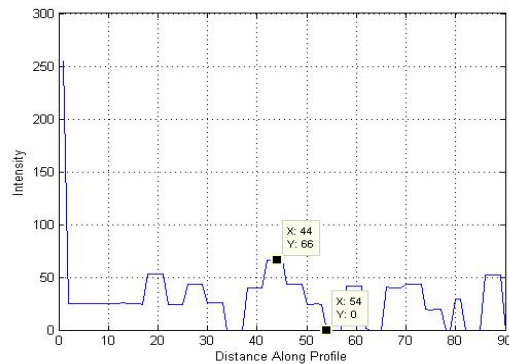


Figure 5.4.7(d)

Figure 5.4.7(a): Raw image with line profile before processing. Figure 5.4.7(b): Raw image intensity profile before processing using TSR. Figure 5.4.7(c): Result image with line profile after TSR processing. Figure 5.4.7(d): Result image intensity profile after processing using TSR processing.

**Discussion:** The Economical SVD based PCT show better processing and intensity variation results compared to the SVD and TSR. For the same number of thermal image sequences the Economical SVD needed least computation time. The Economical SVD based PCT showed higher region of interest selection capability in comparison with the two processing routines. The processed image using TSR showed least variation in contrast between the adhesive and the steel panels. The comparison between the three processing routines is shown in table 5-G and 5-H.

<b>Type</b>	<b>Frame Number</b>	<b>ROI Size</b>	<b>Run Time</b>
Economical SVD	10	340*170	5 sec
SVD	10	100*100	10 sec
TSR	10	100*100	80 sec

Table 5-G: Flash image sequence settings and processing time of the processing routines

<b>Type</b>	<b>Intensity variation of raw image</b>	<b>Intensity variation of processed image</b>
Economical SVD	32	210
SVD	40	213
TSR	40	66

Table 5-H: Flash processing intensity calculations

### 5.5 Thermography using Halogen as Heat Source

The test sample is thermally excited using the halogen lamps in the experimental setup as shown in the figure 5.5.1. The thermal image sequence of the test sample is captured using the thermal imaging camera shown in figure 5.5.1. The captured thermal image sequence is processed using the PCT SVD, Economical SVD and TSR processing routines and the processing results are compared. In all the three processing routines the thermal image sequences are loaded into their respective programs and Region of Interest (ROI) of the thermal image sequence to be processed is selected. Once the ROI of the thermal image sequence is selected, the processing routines carry out their respective processing techniques to enhance the contrast between the defect and non defect area of the sample.

**Economical SVD PCT:** In the Economical SVD based processing technique the thermal image sequence is loaded in to program and the region with all the three adhesive spots is selected as region of interest as shown in figure 5.5.2(a). The processing routine processes the raw image as shown in figure 5.5.2(b) and the processed image shown in

figure 5.5.2(c) is generated with higher contrast and edge visibility compared to the raw image.

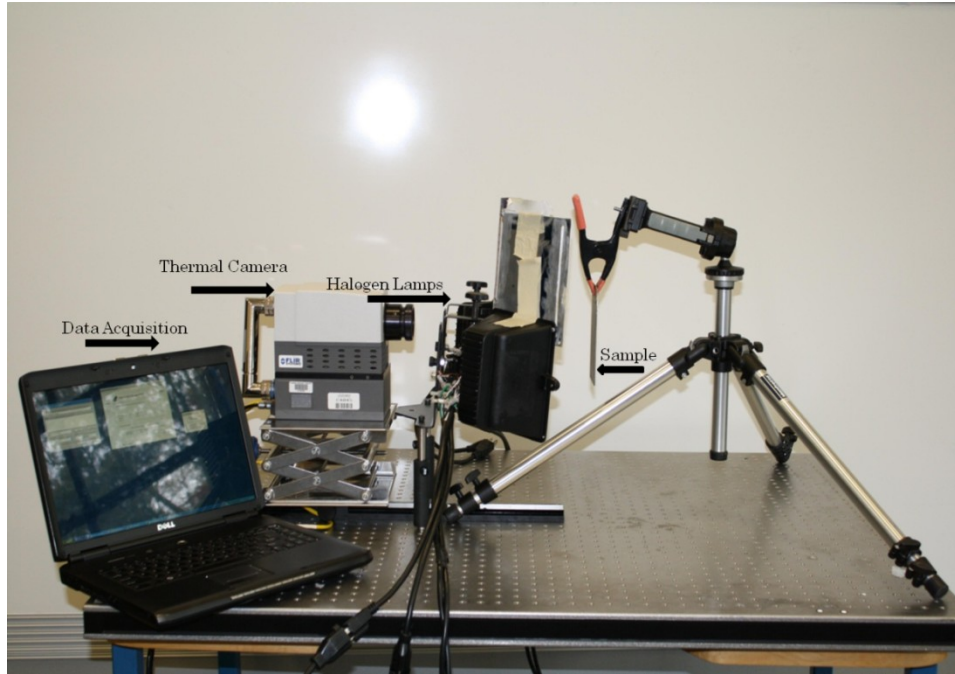


Figure 5.5.1: Halogen Heating Source Experiment

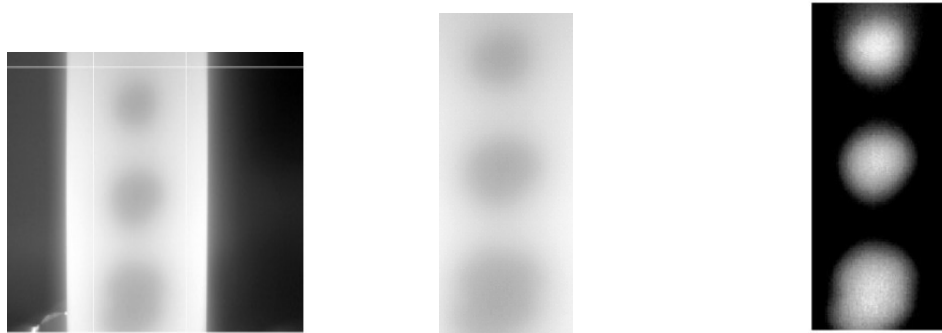


Figure 5.5.2(a)

Figure 5.5.2(b)

Figure 5.5.2(c)

Figure 5.5.2: Economical SVD based PCT Processing and Results of test sample using Halogen Heat Source. Figure 5.5.2(a): ROI of Economical SVD based PCT. Figure 5.5.2(b): Raw image before processing using Economical SVD based PCT. Figure 5.5.2(c): Result image of Economical SVD based Processing.

*Profile Intensity Calculation:* The intensity between the defect and non defect area of the sample is calculated by drawing a line profile from one end of the ROI to the other end as shown in the figure 5.5.3(a). The calculated intensity is plotted along the distance of the profile of sample as shown in the figure 5.5.3(b). Similar to the raw image, the line profile of the processed image is drawn as shown in the figure 5.5.3(c) and the calculated intensity for the line profile is plotted as shown in figure 5.5.3(d). The intensity variation observed in the processed image is much higher than that of the raw image.

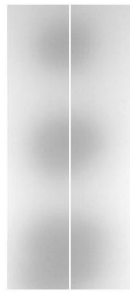


Figure 5.5.3(a)

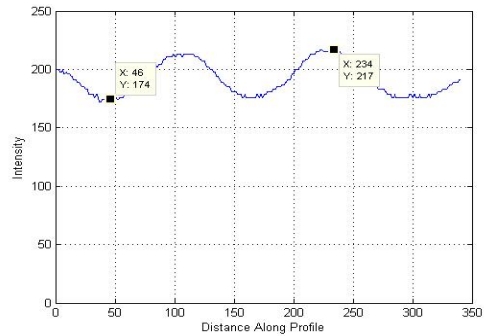


Figure 5.5.3(b)

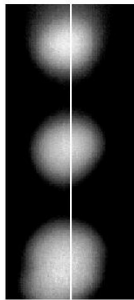


Figure 5.5.3(c)

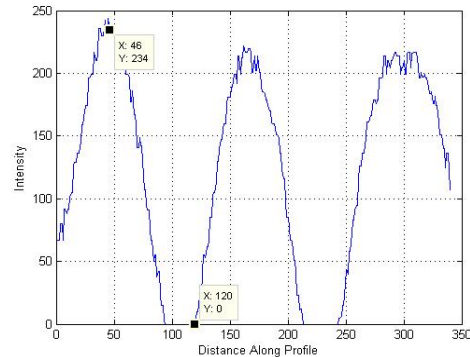


Figure 5.5.3(d)

Figure 5.5.3(a): Raw image with line profile before processing. Figure 5.5.3(b): Raw image intensity profile before processing using Economical SVD based PCT. Figure 5.5.3(c): Result image with line profile after Economical SVD based PCT processing. Figure 5.5.3(d): Result image intensity profile after processing using Economical SVD based PCT processing.

**SVD based PCT:** In the SVD based processing technique the thermal image sequence is loaded in to program and one adhesive spot is selected as region of interest as shown in figure 5.5.4(a) due to processing limitations of the routine. The processing routine processes the raw image as shown in figure 5.5.4(b) and the processed image shown in figure 5.5.4(c) is generated with higher contrast and edge visibility compared to the raw image.

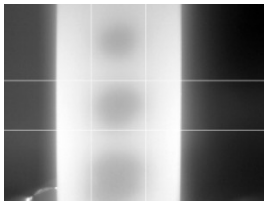


Figure 5.5.4(a)



Figure 5.5.4(b)

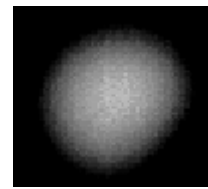


Figure 5.5.4(c)

Figure 5.5.4: SVD based PCT Processing and Results of test sample using Halogen Heat Source. Figure 5.5.4(a): ROI of SVD based PCT. Figure 5.5.4(b): Raw image before processing using SVD based PCT. Figure 5.5.4(c): Result image of SVD based Processing.

*Profile Intensity Calculation:* The intensity between the defect and non defect area of the sample is calculated by drawing a line profile from one end of the ROI to the other end as shown in the figure 5.5.5(a). The calculated intensity is plotted along the distance of the profile of sample as shown in the figure 5.5.5(b). Similar to the raw image, the line profile of the processed image is drawn as shown in the figure 5.5.5(c) and the calculated intensity for the line profile is plotted as shown in figure 5.5.5(d). The intensity variation observed in the processed image is similar to that obtained using economical SVD.



Figure 5.5.5(a)

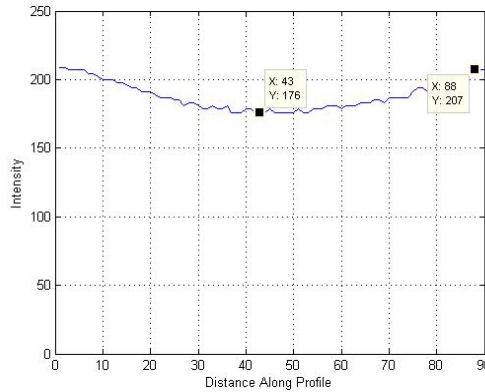


Figure 5.5.5(b)

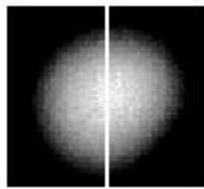


Figure 5.5.5 (c)

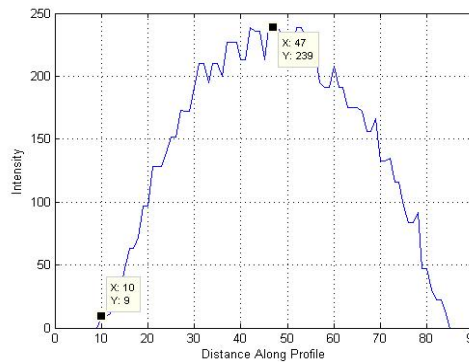


Figure 5.5.5(d)

Figure 5.5.5(a): Raw image with line profile before processing. Figure 5.5.5(b): Raw image intensity profile before processing using SVD based PCT. Figure 5.5.5(c): Result image with line profile after SVD based PCT processing. Figure 5.5.5(d): Result image intensity profile after processing using SVD based PCT processing.

**Thermal Signal Reconstruction (TSR):** In the TSR based processing technique the thermal image sequence is loaded in to program and the region with one adhesive spot is selected as region of interest as shown in figure 5.5.6(a). The processing routine processes the raw image as shown in figure 5.5.6(b) and the processed image shown in figure 5.5.6(c) does not show any contrast variation between the defect and non defect area.



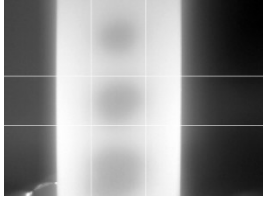


Figure 5.5.6(a)



Figure 5.5.6(b)



Figure 5.5.6(c)

Figure 5.5.6: TSR Processing and Results of test sample using Halogen Heat Source.  
 Figure 5.5.6(a): ROI of TSR. Figure 5.5.6(b): Raw image before processing using TSR.  
 Figure 5.5.6(c): Result image of TSR Processing.

*Profile Intensity Calculation:* The intensity between the defect and non defect area of the sample is calculated by drawing a line profile from one end of the ROI to the other end as shown in the figure 5.5.7(a). The calculated intensity is plotted along the distance of the profile of sample as shown in the figure 5.5.7(b). Similar to the raw image, the line profile of the processed image is drawn as shown in the figure 5.5.7(c) and the calculated intensity for the line profile is plotted as shown in figure 5.5.7(d). The intensity variation is degraded with the use of TSR as it is not developed to be used on halogen or steady state heating.



Figure 5.5.7(a)

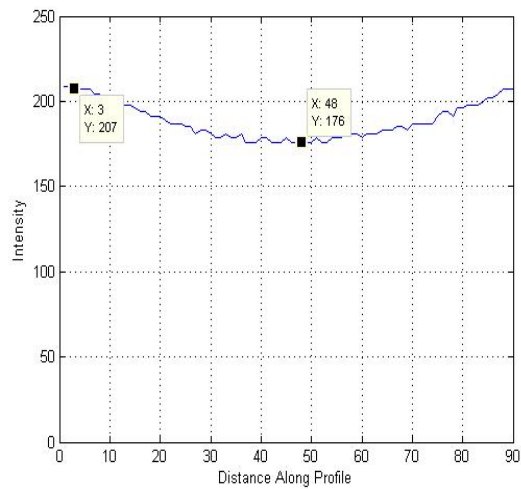


Figure 5.5.7(b)



Figure 5.5.7(c)

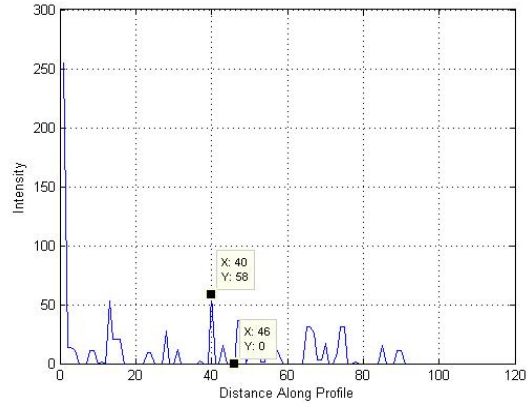


Figure 5.5.7(d)

Figure 5.5.7(a): Raw image with line profile before processing. Figure 5.5.7(b): Raw image intensity profile before processing using TSR. Figure 5.5.7(c): Result image with line profile after TSR processing. Figure 5.5.7(d): Result image intensity profile after processing using TSR processing.

**Discussion:** The Economical SVD based PCT generated better processing and intensity variation results compared to the SVD and TSR. The computation time needed for Economical SVD is least in comparison with both SVD and TSR techniques. The region of interest selected using Economical SVD based PCT is also higher than the other two processing routines. There is no contrast variation evaluated between the defect and non defect area using the TSR processing technique. The comparison of three processing routines is shown in table 5-I and 5-J.

Type	Frame Number	ROI Size	Run Time
Economical SVD	10	360*110	5 sec
SVD	10	100*100	10 sec
TSR	10	100*100	50 sec

Table 5-I: Halogen image sequence settings and processing time of the processing routines

Type	Intensity variation of raw image	Intensity variation of processed image
Economical SVD	43	234
SVD	31	230
TSR	31	58

Table 5-J: Halogen processing intensity calculations

### 5.6 Thermography using Induction as Heat Source

The test sample is thermally using the induction coil as mentioned in the previous section. The thermal image sequence of the test sample is captured using thermal imaging camera. The captured thermal image sequence is processed using the PCT SVD, Economical SVD and TSR processing routines and the processing results are compared. In all the three processing routines the thermal image sequences are loaded into their respective programs and Region of Interest (ROI) of the thermal image sequence to be processed is selected. Once the ROI of the thermal image sequence is selected, the processing routines carry out their respective processing techniques to enhance the contrast between the defect and non defect area of the sample.

**Economical SVD PCT:** In the Economical SVD based processing technique the thermal image sequence is loaded in to program and the region with all the three adhesive spots is selected as region of interest as shown in figure 5.6.1(a). The processing routine processes the raw image as shown in figure 5.6.1(b) and the processed image shown in figure 5.6.1(c) is generated with higher constrast and edge visibility compared to the raw image.

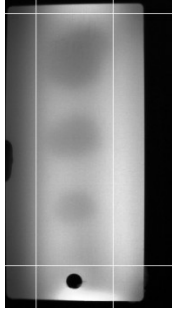


Figure 5.6.1(a)

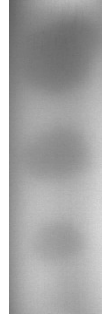


Figure 5.6.1(b)

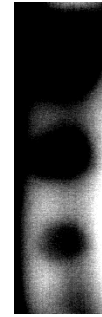


Figure 5.6.1(c)

Figure 5.6.1: Economical SVD based PCT Processing and Results of test sample using Induction Heat Source. Figure 5.6.1(a): ROI of Economical SVD based PCT. Figure 5.6.1(b): Raw image before processing using Economical SVD based PCT. Figure 5.6.1(c): Result image of Economical SVD based Processing.

*Profile Intensity Calculation:* The intensity between the defect and non defect area of the sample is calculated by drawing a line profile from one end of the ROI to the other end as shown in the figure 5.6.2(a). The calculated intensity is plotted along the distance of the profile of sample as shown in the figure 5.6.2(b). Similar to the raw image, the line profile of the processed image is drawn as shown in the figure 5.6.2(c) and the calculated intensity for the line profile is plotted as shown in figure 5.6.2(d). The intensity variation observed in the processed image is much higher than that of the raw image.



Figure 5.6.2(a)

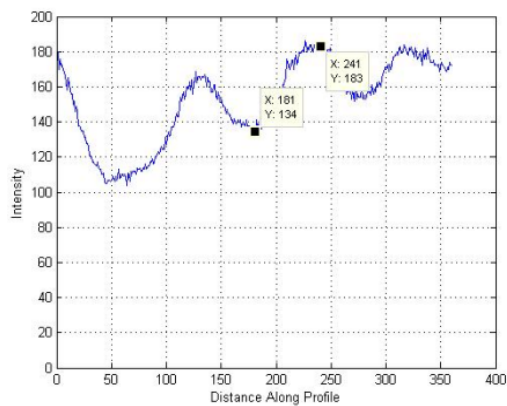


Figure 5.6.2(b)

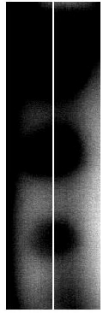


Figure 5.6.2(c)

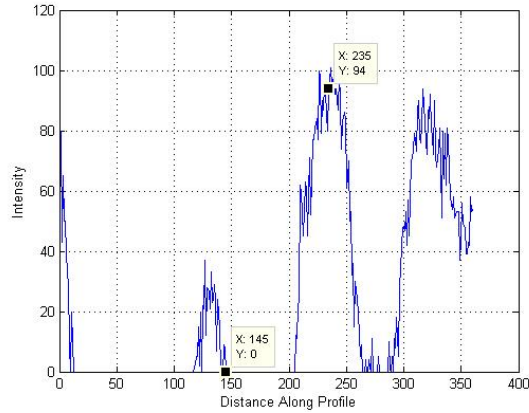


Figure 5.6.2(d)

Figure 5.6.2(a): Raw image with line profile before processing. Figure 5.6.2(b): Raw image intensity profile before processing using Economical SVD based PCT. Figure 5.6.2(c): Result image with line profile after Economical SVD based PCT processing. Figure 5.6.2(d): Result image intensity profile after processing using Economical SVD based PCT processing.

**SVD based PCT:** In the SVD based processing technique the thermal image sequence is loaded in to program and the region with one adhesive spot is selected as region of interest as shown in figure 5.6.3(a) due to processing limitations of the routine. The processing routine processes the raw image as shown in figure 5.6.3(b) and the processed image shown in figure 5.6.3(c) is generated with higher contrast and edge visibility compared to the raw image.

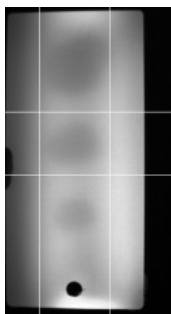


Figure 5.6.3(a)



Figure 5.6.3(b)

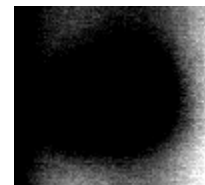


Figure 5.6.3(c)

Figure 5.6.3: SVD based PCT Processing and Results of test sample using Induction Heat Source. Figure 5.6.3(a): ROI of SVD based PCT. Figure 5.6.3(b): Raw image before processing using SVD based PCT. Figure 5.6.3(c): Result image of SVD based Processing.

*Profile Intensity Calculation:* The intensity between the defect and non defect area of the sample is calculated by drawing a line profile from one end of the ROI to the other end as shown in the figure 5.6.4(a). The calculated intensity is plotted along the distance of the profile of sample as shown in the figure 5.6.4(b). Similar to the raw image, the line profile of the processed image is drawn as shown in the figure 5.6.4(c) and the calculated intensity for the line profile is plotted as shown in figure 5.6.4(d). The intensity variation observed in the processed image is similar to that obtained using economical SVD but it can be used only to smaller ROI.



Figure 5.6.4(a)

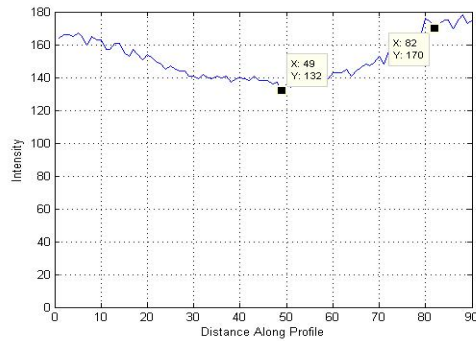


Figure 5.6.4(b)

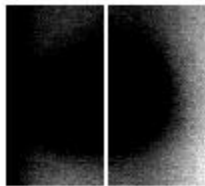


Figure 5.6.4 (c)

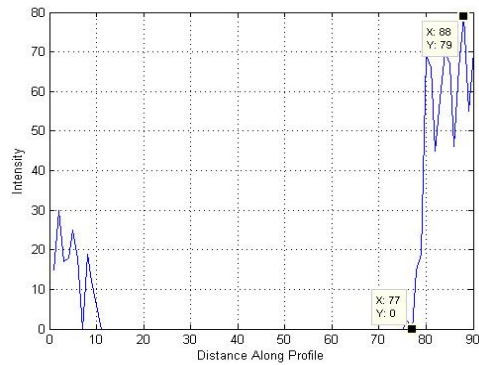


Figure 5.6.4(d)

Figure 5.6.4(a): Raw image with line profile before processing. Figure 5.6.4(b): Raw image intensity profile before processing using SVD based PCT. Figure 5.6.4(c): Result image with line profile after SVD based PCT processing. Figure 5.6.4(d): Result image intensity profile after processing using SVD based PCT processing

**Thermal Signal Reconstruction (TSR):** In the TSR based processing technique the thermal image sequence is loaded in to program and the region with one adhesive spots is selected as region of interest as shown in figure 5.6.5(a). The processing routine processes the raw image as shown in figure 5.6.5(b) and the processed image shown in figure 5.6.5(c) does not show any contrast variation between the defect and non defect area.

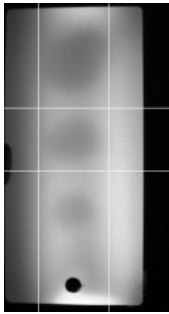


Figure 5.6.5(a)



Figure 5.6.5(b)



Figure 5.6.5(c)

Figure 5.6.5: TSR Processing and Results of test sample using Induction Heat Source. Figure 5.6.5(a): ROI of TSR. Figure 5.6.5(b): Raw image before processing using TSR. Figure 5.6.5(c): Result image of TSR Processing.

*Profile Intensity Calculation:* The intensity between the defect and non defect area of the sample is calculated by drawing a line profile from one end of the ROI to the other end as shown in the figure 5.5.6(a). The calculated intensity is plotted along the distance of the profile of sample as shown in the figure 5.5.6(b). Similar to the raw image, the line profile of the processed image is drawn as shown in the figure 5.5.6(c) and the calculated intensity for the line profile is plotted as shown in figure 5.5.6(d). The intensity variation

observed in the processed image like noise captured in the image sequence along with the useful thermographic data. The processing degrades the initial of the captured image sequence.

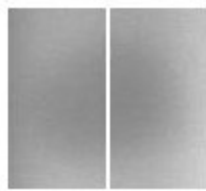


Figure 5.5.6(a)

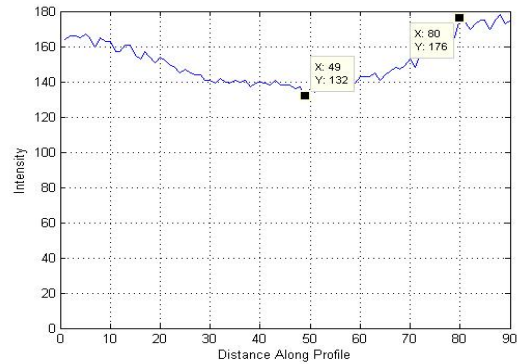


Figure 5.5.6(b)



Figure 5.5.6(c)

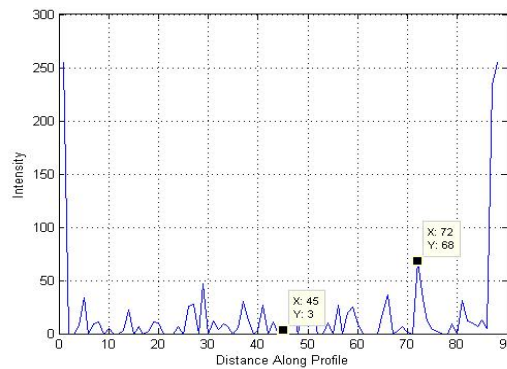


Figure 5.5.6(d)

Figure 5.5.6(a): Raw image with line profile before processing. Figure 5.5.6(b): Raw image intensity profile before processing using TSR. Figure 5.5.6(c): Result image with line profile after TSR processing. Figure 5.5.6(d): Result image intensity profile after processing using TSR processing.

**Discussion:** The Economical SVD based PCT show better contrast between the steel panels and adhesive in comparison with SVD and TSR. For the same number of thermal image sequences the Economical SVD needed least computation time along with the capability to select larger region of interest of the sample. There is no contrast variation



the defect and non defect are in the TSR processing technique. The comparison of three processing routines is shown in table 5-K and 5-L.

<b>Type</b>	<b>Frame Number</b>	<b>ROI Size</b>	<b>Run Time</b>
Economical SVD	10	340*150	5 sec
SVD	10	100*100	10 sec
TSR	10	100*100	55 sec

Table 5-K: Induction image sequence settings and processing time of the processing routines

<b>Type</b>	<b>Intensity variation of raw image</b>	<b>Intensity variation of processed image</b>
Economical SVD	49	94
SVD	38	88
TSR	44	68

Table 5-L: Induction processing intensity calculations

## Chapter 6

### Conclusion and Future Work

The step by step procedure of implementing the proposed Economical Singular Value Decomposition (SVD) based PCT technique is explained. The proposed Economical SVD is applied on the thermographic image sequences obtained using various thermal excitation techniques such as the halogen, pulse and induction. The processed image sequences showed good contrast variation between the steel panels and adhesive used for joining them in comparison with the conventional thermographic computation routines such as the Thermal Signal Reconstruction technique. The proposed processing routine showed good contrast enhancement and edge detect ability to a larger region of interest used for processing with less computation time needed in comparison with the available techniques such as the Singular Value Decomposition and Thermal Signal Reconstruction techniques. The benchmarking of the proposed technique with conventional routines is done using similar experimental and computation settings. In the bench marking, the proposed technique being generic in nature provided us with promising results on thermographic data generated using various thermal excitation sources which is not the case with the conventional routines which are source specific.

**Future work** include, the identification of the procedure to quantify the depth and width information of the defect using the temperature time history from the IR image sequences. The processing lacks some crispness when the sample is heated using induction heat source which is to be investigated. Samples with composite materials and sandwich structures are to be inspected and processed using the proposed technique.

### List of References

1. Maldague X.P. (2001). Theory & practice of infrared technology for nondestructive testing. John Wiley & Sons.
2. Brett J.I. (2008). Selecting a Non-Destructive Method, Part IV: Thermal/Infrared Inspection Techniques-Thermography. The Ammtiac Quarterly, Volume 3 Number 2.
3. Passive Thermographic Imaging Shows Promise for Detecting Hidden Corrosion. (2008). [http://www.ml.afrl.af.mil/stories/MLL/asc\\_04\\_0163.html](http://www.ml.afrl.af.mil/stories/MLL/asc_04_0163.html).
4. Shepard S. (2006). Understanding Flash Thermography. Materials Evaluation, 460-464.
5. Castanedo I.C, Piau J.M, Guilbert S, Avdelidis N.P, Genest M, Bendada A, Maldague X.P.V. (2009). Comparative study of active thermography techniques for the nondestructive evaluation of honeycomb structures. Research in Nondestructive Evaluation, 1–31.
6. Meola C, Carlomagno G.M, Squillace A, Giorleo G. (2004). The use of infrared thermography for nondestructive evaluation of joints. Infrared Physics & Technology 46, 93–99.
7. Castanedo C.I, Grinzato E, Marinetti S, Bison P, Avdelidis N, Grenier M, Piau J.M, Bendada A and Maldague X. (2008). Quantitative assessment of aerospace materials by active thermography Techniques. 9th International Conference on Quantitative InfraRed Thermography.  
[http://www.thermo.p.lodz.pl/qirt/abstracts/QIRT2008\\_Ibarra\\_et\\_al.pdf](http://www.thermo.p.lodz.pl/qirt/abstracts/QIRT2008_Ibarra_et_al.pdf)
8. Mendioroz A, Apiñaniz E, Salazar A, Venegas P and S´aez-Oc´ariz I. (2009). Quantitative study of buried heat sources by lock-in vibrothermography: an

- approach to crack characterization. *Journal of Physics D: Applied Physics*, 8 pages.
9. Mendioroz A, Apiñaniz E, Salazar A, Venegas P and S´aez-Oc´ariz I. (2008). Crack Characterization in metallic plates using vibrothermography. 9th International Conference on Quantitative Infrared Thermography.
  10. Rogalski A, Chrzanowski K. (2002). Infrared devices and techniques. *Opto-Electronics Review*. 111-136.
  11. Hristov N.I, Betke M, Kunz T.H. (2008). Applications of thermal infrared imaging for research in aero ecology. *Integrative and Comparative Biology*. 1-10.
  12. Shepard S. (2007). Thermography of Composites. *Materials Evaluation*. 690-696.
  13. Castanedo C.I, Bendada A, Maldague X. (2007). Thermographic Image Processing for NDT. IV Conferencia Panamericana de END, Buenos Aires.
  14. Maldague X, Marinetti S. (1996). Pulse phase infrared thermography. *Journal of Applied Physics*, 2694-2698
  15. Almond D.P, Lau S.K. (1994). Defect sizing by transient thermography. I: An analytical treatment. *J. Phys. D: Applied Physics*, 1063-1069.
  16. A quantitative review of three flash thermography processing routines. *Infrared Physics & Technology* 51 (2008) 300–306. Mohammed A. Omar, Yi Zhou
  17. Michael E.W, Andreas R, Luis M.R. (2002). Singular Value Decomposition and principal component analysis for gene expression analysis. Modeling, Algorithms and Informatics Group (CCS-3) Los Alamos National Laboratory.

18. Rajic N. (2002). Principal component thermography for flaw contrast enhancement and flaw depth characterisation in composite structures. *Composite Structures* 58, 521–528.
19. Rajic N. (2002). Principal component thermography. DSTO Aeronautical and Maritime Research Laboratory.
20. Marinetti S , Grinzato E , Bison P.G , Bozzi E, Chimenti M , Pieri G, Salvetti O.(2004). Statistical analysis of IR thermographic sequences by PCT, *Infrared Physics & Technology* 46, 85–91.